

Indian and Pacific Ocean Influences on Southeast Australian Drought and Soil Moisture

CAROLINE C. UMMENHOFER,* ALEXANDER SEN GUPTA,* PETER R. BRIGGS,+
MATTHEW H. ENGLAND,* PETER C. MCINTOSH,# GARY A. MEYERS,@ MICHAEL J. POOK,#
MICHAEL R. RAUPACH,+ AND JAMES S. RISBEY#

* *Climate Change Research Centre, University of New South Wales, Sydney, New South Wales, Australia*

+ *Centre for Australian Weather and Climate Research, Canberra, Australian Capital Territory, Australia*

@ *CSIRO Marine and Atmospheric Research, and Institute of Marine and Antarctic Research,
University of Tasmania, Hobart, Tasmania, Australia*

(Manuscript received 16 October 2009, in final form 27 May 2010)

ABSTRACT

The relative influences of Indian and Pacific Ocean modes of variability on Australian rainfall and soil moisture are investigated for seasonal, interannual, and decadal time scales. For the period 1900–2006, observations, reanalysis products, and hindcasts of soil moisture during the cool season (June–October) are used to assess the impacts of El Niño–Southern Oscillation (ENSO) and the Indian Ocean dipole (IOD) on southeastern Australia and the Murray–Darling Basin, two regions that have recently suffered severe droughts. A distinct asymmetry is found in the impacts of the opposite phases of both ENSO and IOD on Australian rainfall and soil moisture. There are significant differences between the dominant drivers of drought at interannual and decadal time scales. On interannual time scales, both ENSO and the IOD modify southeastern Australian soil moisture, with the driest (wettest) conditions over the southeast and more broadly over large parts of Australia occurring during years when an El Niño and a positive IOD event (La Niña and a negative IOD event) co-occur. The atmospheric circulation associated with these responses is discussed. Lower-frequency variability over southeastern Australia, however, including multiyear drought periods, seems to be more robustly related to Indian Ocean temperatures than Pacific conditions. The frequencies of both positive and negative IOD events are significantly different during periods of prolonged drought compared to extended periods of “normal” rainfall. In contrast, the frequency of ENSO events remains largely unchanged during prolonged dry and wet periods. For the Murray–Darling Basin, there appears to be a significant influence by La Niña and both positive and negative IOD events. In particular, La Niña plays a much more prominent role than for more southern regions, especially on interannual time scales and during prolonged wet periods. For prolonged dry (wet) periods, positive IOD events also occur in unusually high (low) numbers.

1. Introduction

Australian climate is characterized by arid to semi-arid conditions for large parts of the continent. Such conditions are prone to large interannual and longer-term rainfall variability with frequent, pronounced dry spells, often persisting for a decade or longer. Even so, the severity of the drought experienced currently across southeastern Australia (SEA) seems exceptional in its intensity (Sohn 2007; Murphy and Timbal 2008). The

severely affected Murray–Darling Basin (MDB) is home to Australia’s largest river system, with about 65% of the country’s irrigation and approximately 40% of the total Australian agricultural production taking place there (ABARE 2009). However, over the last decade, inflows into the Murray River system were 44% below the long-term average (CSIRO 2010). This has resulted in unprecedented socioeconomic and environmental impacts for the region with rural and metropolitan water restrictions, declines in agricultural production, far-reaching damage to the various ecosystems, and increased risk of bushfires (LeBlanc et al. 2009). The drought presently affecting SEA is “one of the most severe observed recently in the world” (LeBlanc et al. 2009) and has been dubbed the “Big Dry” (Sohn 2007). Yet,

Corresponding author address: Caroline Ummenhofer, Climate Change Research Centre, University of New South Wales, Sydney, NSW 2052, Australia.
E-mail: c.ummenhofer@unsw.edu.au

causes of the Big Dry are still widely debated and a better understanding of the factors influencing multiyear drought cycles across SEA is warranted.

The latest SEA drought has been accompanied by sustained long-term declines in precipitation across southern regions of Australia, with the majority of the decrease over SEA occurring during late austral autumn (e.g., Murphy and Timbal 2008, and references therein). Cai and Cowan (2008a) linked this autumn rainfall decline to changes in the El Niño–Southern Oscillation (ENSO), more specifically an increased (decreased) frequency of El Niño (La Niña) events. This coincided with a reduction in rain-bearing northwest cloud bands resulting from changes in atmospheric wave trains associated with subtropical Indian Ocean SST anomaly patterns, possibly due to long-term Indian Ocean warming (Cai and Cowan 2008a). During austral winter and spring, Cai et al. (2009) suggested that the higher frequency of positive Indian Ocean dipole (IOD) events since the 1950s could potentially account for a large proportion of the SEA rainfall reduction during that season. In contrast, Nicholls (2009) linked the autumn rainfall trend to increases in pressure over Australia, possibly driven by the positively trending southern annular mode (SAM): in excess of 70% of the observed rainfall decrease could be accounted for by the trend in the SAM. Previous studies (Hendon et al. 2007; Meneghini et al. 2007) also suggested that trends in the SAM could have contributed toward rainfall trends across southern regions of Australia for some seasons. Murphy and Timbal (2008) proposed that pressure increases, both large scale (i.e., associated with trends in the SAM) and regional (i.e., due to trends in the subtropical ridge), may have contributed to a decrease in the number and impact of rain-bearing midlatitude systems over SEA. Because of the strong relationship between local pressure and precipitation, Hope et al. (2009) also suggested that the rainfall decline is related to long-term increases in pressure over southern Australia.

Previous studies mostly saw the present severe multiyear drought conditions as the culmination of the long-term decline in rainfall. In contrast, Ummenhofer et al. (2009a) assessed prolonged drought periods in SEA over the past 120 years and found them to be strongly linked to Indian Ocean variability. More specifically, a conspicuous absence of the negative phase of the IOD (Saji et al. 1999; Webster et al. 1999) deprived SEA of its normal rainfall quota throughout all the major iconic droughts of the twentieth century, including the most recent Big Dry. The present study builds on this previous work by taking an integrated view of the hydrological conditions across SEA, assessing both atmospheric and terrestrial branches and the links to

ENSO and IOD during prolonged droughts over the past century.

On interannual time scales, SEA precipitation is modulated by both of these tropical climate modes. As the dominant coupled mode of tropical Pacific Ocean variability, ENSO exerts a considerable influence on Australian climate. Traditionally, ENSO has been seen as a driver of both rainfall variability (e.g., Ropelewski and Halpert 1987; Drosowsky and Williams 1991, and references therein) and severe droughts (e.g., Nicholls 1988; Wang and Hendon 2007). ENSO's influence is strongest over eastern and northeastern regions of Australia, especially in winter and spring (Risbey et al. 2009b, and references therein). However, SEA is also significantly affected by ENSO events on interannual time scales. Furthermore, variations between different types, or "flavors," of El Niño events have recently gained attention with the recognition that these different flavors can induce very different precipitation responses across the Pacific region in general (Ashok et al. 2007; Weng et al. 2007) and Australia in particular (Wang and Hendon 2007; Brown et al. 2009; Taschetto and England 2009; Taschetto et al. 2009). Teasing apart such complex relationships and teleconnection patterns is further hampered by the frequent co-occurrence of ENSO and IOD, a consequence of ENSO being at least a partial driver of IOD variability.

The IOD is characterized by an out-of-phase relationship between equatorial sea surface temperatures (SSTs) in the eastern and western Indian Ocean and a coincident reorganization of the large-scale atmospheric circulation (Saji et al. 1999; Webster et al. 1999). Being strongly phase locked to the seasonal cycle, the IOD mainly affects rainfall across western and southern regions of Australia during winter and spring. During a positive IOD, dry conditions are more prevalent over southern Australia due to an anomalous anticyclonic circulation at low levels over the eastern tropical and subtropical Indian Ocean (Ashok et al. 2003). In model simulations, Ummenhofer et al. (2009b) found that enhanced meridional SST gradients across the eastern Indian Ocean as seen during negative IOD events led to a matching pattern of changes in the thickness gradient. The resulting thermal wind response strengthened the onshore moisture advection causing anomalous wet conditions over western and southern Australia. Similarly, negative IOD years over the last 120 years have been characterized by enhanced tropical moisture flux and consistently above-average rainfall over SEA (Ummenhofer et al. 2009a).

The frequent co-occurrence and widely debated degree of dependence of the IOD on Pacific forcing highlight the importance of separating the relative impacts

of these climate drivers on Australian precipitation. Several studies have assessed the interactions and relative influences on Australian interannual precipitation of the two bordering tropical ocean basins (Meyers et al. 2007; Risbey et al. 2009a,b). In particular, Meyers et al. (2007) devised a classification to distinguish independent and co-occurring ENSO and IOD events. They found distinct rainfall patterns across Australia for “pure” and combined ENSO–IOD events, highlighting the atmosphere’s sensitivity to small SST changes in both the Pacific and Indian Ocean basins. Risbey et al. (2009a) used this ENSO–IOD classification to assess differences in the synoptic situation over SEA. During years with co-occurring La Niña and negative IOD, an enhanced meridional thickness gradient favorable for cutoff low pressure system formation and increased rainfall were observed over SEA. The opposite occurred during years with an El Niño and positive IOD event (Risbey et al. 2009a).

Adding a further level of complexity, these teleconnection patterns are not stationary in time, but vary on decadal time scales and beyond. ENSO’s influence on Australian precipitation varies on multidecadal time scales depending on the phase of the Interdecadal Pacific Oscillation (IPO; Power et al. 1999a). When the IPO is in its positive phase, with warmer equatorial Pacific SSTs, the relationship between ENSO and Australian rainfall is weak, compared to periods of negative IPO. Similarly, Arblaster et al. (2002) found a weakened relationship between Australian rainfall and ENSO during such decadal periods of positive tropical Pacific SST anomalies related to a flattening in the slope in the equatorial thermocline with an associated reduction in ENSO variability. Decadal variability in the Indian Ocean was also found to modulate rainfall over eastern Australia (Power et al. 1999a). A decadal signal in the strength of the IOD has also been identified in observations (Ashok et al. 2004) and model simulations (Tozuka et al. 2007), with possible impacts on the climate of the surrounding landmasses. Due to the interaction of ENSO and IOD on longer time scales, it is important to also investigate decadal variations spanning the full Indo-Pacific region. D’Arrigo et al. (2011) investigated long-term variability across the tropical Indo-Pacific system and the response for Indonesian climate from paleoproxy records. They found periods of suppressed/enhanced tropical variability to be coherent in both ocean basins. By partitioning years into neutral, “pure,” and combined ENSO–IOD years, we will explore here how the impacts of the tropical Indo-Pacific system on Australian precipitation vary on interannual and longer time scales and how this relates to prolonged dry and wet periods in SEA, focusing on the cool season (June–October). It is this period when rainfall

is of most importance to the major agricultural enterprises such as grains and dairy.

The interconnection between the tropical Indian and Pacific system calls for a combined assessment of their impacts on precipitation over eastern Australia. Variations in the interaction of ENSO and the IOD on different time scales, from seasonal to interannual and decadal, suggest that teleconnection patterns linked to these modes might also vary. For this purpose, we introduce the concept of “intervals,” that is, prolonged multiyear periods of anomalous dry and wet conditions, in addition to the more commonly used approach of interannual variability. Specifically, it is of interest to explore whether the influences that ENSO and IOD have on Australian rainfall are the same on both the year-to-year time scales and also during these intervals or lower-frequency time slices. Though not explicit, this approach of intervals was employed by Ummenhofer et al. (2009a) to investigate prolonged droughts over SEA. Here, we expand on this previous work by including both prolonged dry and wet periods. Furthermore, the spatial domain is extended to contrast results obtained for SEA with those for the MDB.

A key emergent issue within this context is nonlinearity across spatial and temporal scales. In regard to temporal aspects, we explore whether the dominance of a particular driver of Australian hydrology is dependent on the time scale examined. Decadal modulation, as discussed above, of the impact of ENSO on Australian rainfall and its predictability (e.g., Power et al. 2006) add extra complexity to this temporal nonlinearity. Furthermore, we assess whether the interaction of ENSO and IOD causes a linear spatial response. In other words, is the anomalous precipitation observed during a year with co-occurring El Niño and positive IOD equivalent to the sum of the anomalies during individual events? The key objective of this study is to explore the relative influence of ENSO and IOD on Australian hydrology across a range of temporal scales to assess whether such spatial and temporal nonlinearities exist.

To characterize prolonged dry and wet periods, it is advantageous to not only investigate precipitation but also to assess subsurface water availability. It is actually the water deficits in deeper soil layers, more so than precipitation levels, that exert the most significant stress on natural ecosystems and agriculture alike. LeBlanc et al. (2009) highlight the importance of focusing on subsurface water resources when investigating multiyear drought and associated environmental impacts on water resources. During severe droughts, the ongoing loss of deeper water resources can occur even after surface water supplies have dried up. Of the total water lost between 2002 and 2006 over SEA, only 3% of this is related to available surface water, while 83% and 14% were associated

with groundwater storage and soil moisture, respectively (LeBlanc et al. 2009). Across southern Australia in recent years, prolonged and severe soil moisture deficits during the Big Dry resulted in higher mortality in mature native vegetation (Raupach et al. 2009). In many basins, soil moisture represents a major water store. Liu et al. (2009) showed that recent deficits in soil moisture across eastern Australia had more robust spatial and temporal signals than did rainfall deficits. Here, we analyze soil moisture, especially in deeper layers, which reacts more slowly to changes in available surface water as it integrates hydrological effects over longer time scales. This inertia is useful in distinguishing between high-frequency interannual variability in precipitation and the more slowly varying change associated with intervals in the deep soil moisture. Variability across these different time scales will be assessed with respect to influences from the Pacific and Indian Oceans.

The climate system in the Indo-Pacific region has sustained considerable trends over recent decades. Ocean temperatures in both the tropical Indian and Pacific Oceans have been rising, with profound consequences for the large-scale atmospheric circulation across the region (e.g., Vecchi et al. 2006; Vecchi and Soden 2007; Power and Smith 2007; Abram et al. 2008; Ihara et al. 2008). Indisputably, recent higher air temperatures, in addition to substantial rainfall deficits, have exacerbated the drought situation over SEA. Nicholls (2004) found that both the mean maximum and minimum temperatures in this latest drought period are higher than in previous droughts due to continued continental-scale warming since the mid-twentieth century almost certainly caused by increased greenhouse gas concentrations (Karoly and Braganza 2005; Nicholls 2006). Nicholls (2004) raised the possibility that higher temperatures and enhanced evaporation could exacerbate the severity of Australian droughts, even without decreases in rainfall. This is consistent with the marked increases in drought frequency found by Mpelasoka et al. (2008) for future climate projections. Cai and Cowan (2008b) reported a 15% reduction in annual inflow into the MDB due to a 1°C rise in temperatures. Under these exacerbated conditions, the present study can offer insights into the multiple influences affecting the region's rainfall on short- to longer-term time scales.

The remainder of the paper is structured as follows. Section 2 describes the datasets and model used. Section 3 presents the Australian rainfall and soil conditions during ENSO and IOD years. In section 4, variations in the seasonal cycle for southern SEA are presented. For the southern SEA, interannual versus decadal influences are compared in section 5, followed by a comparison of influences. The results for the southern SEA are

contrasted with those for the MDB region in section 6. Finally, section 7 summarizes our main findings.

2. Methods and data

a. Datasets

For observed Australian precipitation and maximum air temperature, we use monthly gridded data at 0.05° resolution from the Australian Bureau of Meteorology (1900–2006; Jones et al. 2009). A focus of this study is on SEA climate and its links to large-scale climate modes. Two regions in SEA are considered here (for details see Fig. 1a):

- 1) the southern most tip of SEA (hereafter called SSEA), defined as the land area south of 35°S between 140° and 150°E, and incorporating the state of Victoria and parts of southern New South Wales and eastern South Australia; this area extends the SEA region defined by Ummenhofer et al. (2009a); and
- 2) the drainage basin of the Murray–Darling River system (hereafter called MDB).

As most of the total annual precipitation in SEA falls during the cooler months, we focus all our analyses on June–October, when the links between ENSO–IOD and SEA rainfall are most pronounced. In addition, these months are the crucial period for the region's dominant agricultural industries, grains and dairy.

To investigate climate conditions during ENSO and IOD events, a suite of reanalysis products are used. Atmospheric circulation anomalies are assessed with data developed jointly by the National Centers for Environmental Prediction (NCEP) and the National Center for Atmospheric Research (NCAR) reanalysis (NNR) project (Kalnay et al. 1996; Kistler et al. 2001). Monthly data are used for the period 1948–2006, though all analyses were checked for robustness by using the shorter period 1957–2006 with improved data quality. In addition, NNR results were compared to those obtained from the 40-yr European Centre for Medium-Range Weather Forecasts (ECMWF) Re-Analysis (ERA-40; Uppala et al. 2005) for the period 1957–2001. If not otherwise indicated, we only show results with NNR due to its more extended data record. The atmospheric variables analyzed include circulation and moisture flux integrated below 500 hPa. Monthly SSTs are taken from the Hadley Centre's Global Sea Ice Coverage and Sea Surface Temperature (HadISST) dataset for the period 1900–2006 (Rayner et al. 2003).

b. ENSO/IOD classification

To assess the relative influences of ENSO and IOD for the period 1900–2006, all years were classified according to the respective state of the Pacific and Indian Oceans.

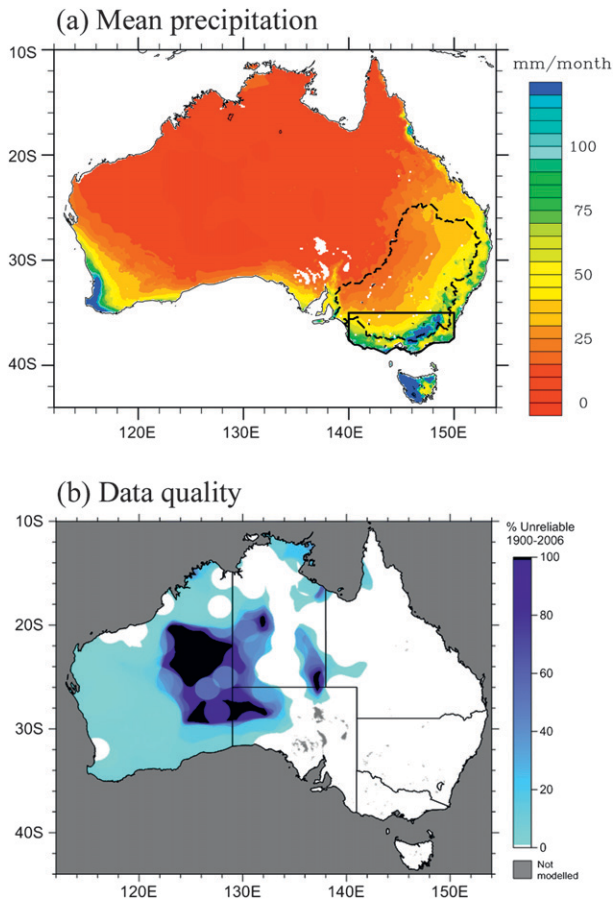


FIG. 1. (a) Australian mean precipitation (mm month^{-1}) averaged for June–October over the period 1900–2006. The spatial extent of the MDB and SSEA are shown by the black dashed and solid lines, respectively. (b) Data quality map for the daily precipitation time series (Jones et al. 2009) used as model forcing for the generation of AWAP soil moisture. The map shows the effects of the expansion (mostly) of the rain gauge network during 1900–2006 on the reliability of the interpolated surfaces, particularly in the west. Gray areas are not modeled due to absent parameter data (oceans, salt lakes, salt pans, inland water, some coastal features). Black areas (100% unreliable) show consistent interpolation failure due to the sparse gauge network in the central and western deserts. White areas are reliable throughout the record within the constraints of the interpolation scheme (Jones et al. 2009). Blue-shaded areas should be treated with varying degrees of caution. For modeling purposes, daily averages calculated from corresponding monthly reanalyses were substituted for areas identified as unreliable in the daily data.

The classification is based on the methodology developed by Meyers et al. (2007) and extended by Ummenhofer et al. (2009a) to 2006. The same classification is used here (Table 1) and has been reproduced from the auxiliary material in Ummenhofer et al. (2009a). As described by Meyers et al. (2007), the classification, though statistical in nature, is physically based. For both ENSO and the IOD, the key process used to classify the two

modes is upwelling. In contrast to earlier classifications, it focuses on the entire Indo-Pacific region, rather than the Pacific Ocean only. Furthermore, the classification is not only reliant on SST data, but also incorporates atmospheric circulation data. It highlights independent events in the Indian Ocean by removing the ENSO signal first. The classification produces a 3×3 matrix of possibilities (Table 1).

For the different ENSO–IOD classifications, composites of June–October SST anomalies are shown as an equivalent 3×3 matrix in Fig. 2. Two combinations, namely a negative IOD (nIOD) co-occurring with an El Niño (EN) event and a La Niña (LN) with a positive IOD (pIOD), occur very rarely in the historic record investigated here, making composite patterns statistically unreliable. As a result, we do not present these combinations. The combined categories, that is, a pIOD coinciding with an El Niño event (Fig. 2b) and an nIOD with a La Niña (Fig. 2f), show generally enhanced SST anomalies compared to the individual or pure categories. This is especially apparent to the northeast and north of Australia around the Indonesian Archipelago, a region that has previously been found to be important for modulating Australian rainfall (e.g., Nicholls 1989; Frederiksen and Balgovind 1994; McIntosh et al. 2007). The key mechanism of upwelling highlighted by Meyers et al. (2007) is seen as anomalously strong upwelling off Java and Sumatra for pIOD events, as coupling between Kelvin waves in the thermocline and the mixed layer SST is a fundamental mechanism in the Bjerknes feedback. The upwelling signature in eastern Indian Ocean SST appears clearly in the map for pIOD (Fig. 2e), but not in the one for El Niño (Fig. 2a). It is worth noting that upwelling also appears in the map for combined El Niño and pIOD events (Fig. 2b). For a more detailed discussion on the SST anomalies in the individual categories, refer to Meyers et al. (2007, and references therein).

c. Australian Water Availability Project

For upper- and lower-layer soil moisture levels, we use gridded monthly estimates of relative soil water content (1900–2006), modeled at 0.05° resolution across the continent as part of the Australian Water Availability Project (AWAP; Raupach et al. 2009).

AWAP uses a simple two-layer dynamic water balance model to determine the state of soil moisture and all water fluxes contributing to changes in soil moisture (precipitation, transpiration, soil evaporation, surface runoff, and deep drainage). The model determines the soil water balance in two layers: soil depths range between 0 and 0.7 m for the upper layer and 0.5 and 1.9 m for the lower layer. Precipitation is a specified forcing flux. Transpiration and soil evaporation are each modeled

TABLE 1. Classification of years when El Niño or La Niña and/or positive or negative IOD events occurred based on a technique designed to highlight independent ENSO and IOD years (Meyers et al. 2007). Also shown are years of neutral conditions. [Table reproduced from Ummenhofer et al. (2009a).]

	nIOD	Neutral	pIOD
El Niño	1930	1877, 1888, 1899, 1905, 1911, 1914, 1918, 1925, 1940, 1941, 1965, 1972, 1986, 1987	1896, 1902, 1957, 1963, 1982, 1991, 1997
Neutral	1915, 1958, 1968, 1974, 1980, 1985, 1989, 1992	1880, 1881, 1882, 1883, 1884, 1895, 1898, 1900, 1901, 1904, 1907, 1908, 1912, 1920, 1921, 1927, 1929, 1931, 1932, 1934, 1936, 1937, 1939, 1943, 1947, 1948, 1951, 1952, 1953, 1959, 1960, 1962, 1966, 1967, 1969, 1971, 1976, 1977, 1979, 1983, 1990, 1993, 1995, 2001, 2002, 2003, 2005, 2006	1885, 1887, 1891, 1894, 1913, 1919, 1923, 1926, 1935, 1944, 1945, 1946, 1961, 1994, 2004
La Niña	1906, 1909, 1916, 1917, 1933, 1942, 1975	1878, 1879, 1886, 1889, 1890, 1892, 1893, 1897, 1903, 1910, 1922, 1924, 1928, 1938, 1949, 1950, 1954, 1955, 1956, 1964, 1970, 1973, 1978, 1981, 1984, 1988, 1996, 1998, 2000	1999

as the lesser of an energy-limited and water-limited value, the energy-limited value is determined from Priestley–Taylor evaporation as an upper-limit evaporation rate at landscape scale in well-watered conditions (Raupach

2000). Both transpiration and soil evaporation are modified for the presence of vegetation using a remotely sensed vegetation cover fraction. Interlayer drainage fluxes are modeled from relative soil moisture using power-law

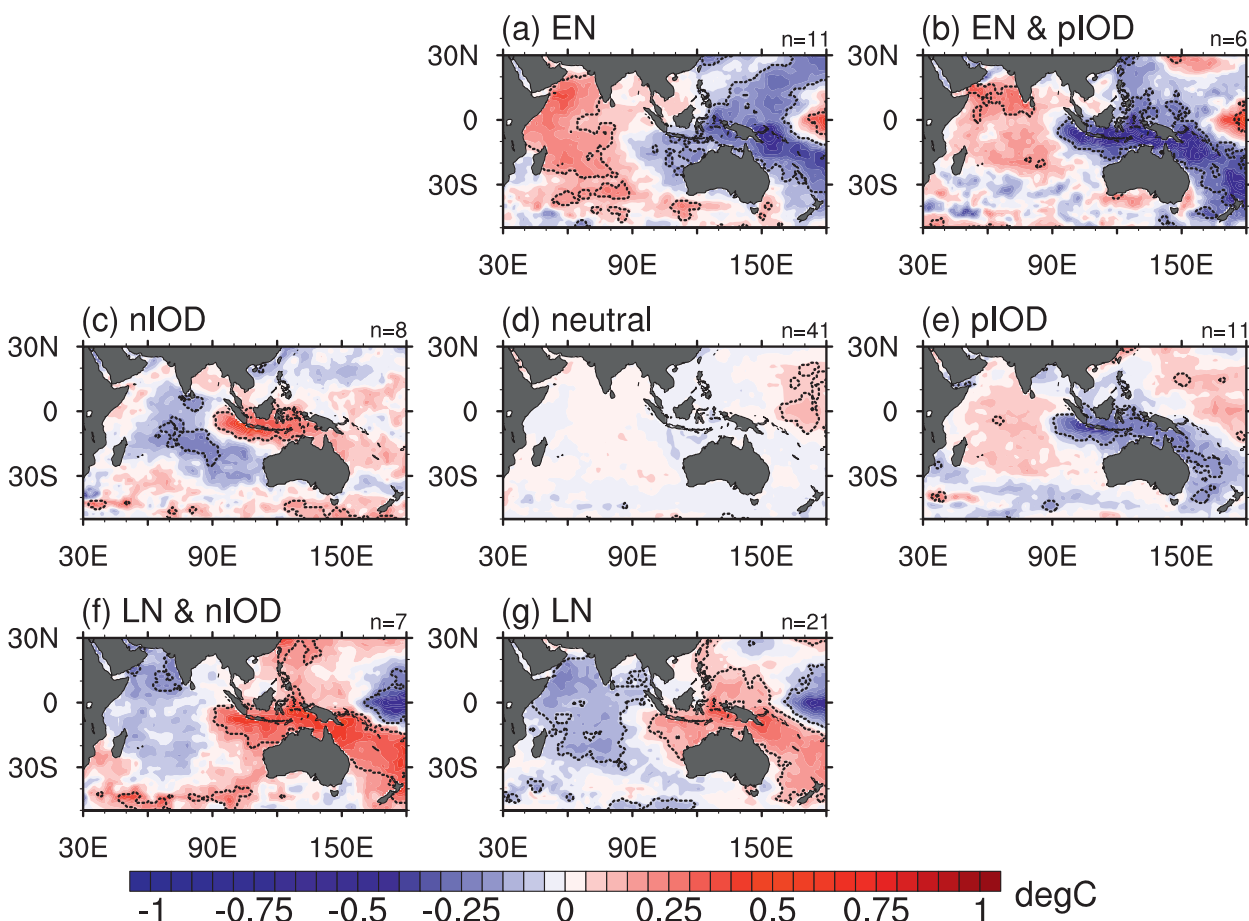


FIG. 2. Composite of the SST anomalies ($^{\circ}\text{C}$) in the different ENSO–IOD categories with the number of members (n) in each category indicated; anomalies are for June–October over the period 1900–2006. The area enclosed by the dashed contours denotes anomalies that are significant at the 90% confidence level as estimated by a two-tailed t test.

formulations. Surface runoff is determined from saturation excess in the upper soil layer, and deep drainage as the drainage outflow from the lower layer. Both surface runoff and deep drainage are treated as fluxes out of the control volume for the soil moisture model into waterways; that is, the water balance is computed in discrete cells without interactions between cells through lateral water transfers [Liang 1994; Liang et al. 1994; similar, e.g., to the variable infiltration capacity (VIC) model].

The model requires inputs of meteorological data (daily precipitation, solar radiation, and maximum and minimum temperatures), soil-layer depths and saturated volumetric water-holding capacities, and vegetation fraction cover. Soil properties are obtained from the Digital Atlas of Australian Soils (McKenzie and Hook 1992; McKenzie et al. 2000). Vegetation is specified using monthly mean maps of the fraction of absorbed photosynthetically active radiation from the Sea-viewing Wide Field-of-view Sensor [SeaWiFS; see Raupach et al. (2009) for details]. The meteorological data are from quality-controlled daily gridded (0.05°) meteorological fields (Jones et al. 2009). Rainfall surfaces are available from 1900 to the present, temperatures from 1910 to the present, and solar radiation from 1990 to the present. To enable soil moisture runs starting in 1900, available monthly climatologies were used as surrogates for daily temperature and solar radiation data where necessary in the earlier part of the record (for temperatures, the period 1900–10 was filled with 1911–40 monthly climatology; for solar radiation, 1900–89 was filled with 1990–2007 monthly climatology). Tests established that soil moisture and water balance results at monthly and longer time scales are insensitive to the replacement of temperature and solar radiation data with monthly climatologies (though results would be sensitive to a similar replacement for precipitation). This shows that our process for constructing a meteorological data record from 1900 to 2007 is satisfactory for the present purpose.

Parameterization and testing of the water balance model is described fully in Raupach et al. (2009). Briefly, the model includes several spatially uniform parameters that were determined by formal parameter estimation methods. Parameters were estimated using a limited test set of observations of total runoff (including both surface runoff and deep drainage) in six unimpaired catchments (without significant water storage or extraction). The parameterized model was then tested against a much wider set of total runoff data from 200 unimpaired catchments. This test produced good agreement except for a small tendency for the model to overpredict total runoff (typically by 2–3 mm yr⁻¹) at low total runoff (≤ 30 mm yr⁻¹).

As a further test, we compared modeled and observed spatial patterns of the surface–air temperature difference over the Murrumbidgee basin (~ 105 km²) in southern New South Wales in two recent years (2005 and 2006). Observed values of this quantity were obtained from the Advanced Along-Track Scanning Radiometer (AATSR) satellite data on land surface temperature and meteorological data, and modeled estimates were obtained by temporally downscaling daily average model predictions to the time of satellite overpass. The agreement in the spatial pattern was good.

Here, we use modeled monthly anomalies of relative soil moisture (defined as a fraction of the saturated water-holding capacity of the soil) in the upper and lower soil layers. For most of our main findings, particularly the relationship between climate drivers (ENSO, IOD) and soil moisture response, we further transform the soil moistures to percentile or decile ranks.

There are several reasons for confidence that the modeled monthly soil moistures are sufficiently reliable for our purposes here. First, the model performance against the tests described above is good. Second, the tests are sensitive: in particular, the relationship between total runoff and precipitation is a strong, nonlinear function that amplifies precipitation variations by a factor of ~ 3 in total runoff, under typical Australian conditions where precipitation is less than potential evaporation (Zhang et al. 2004). This means that the ability of the model to reproduce total runoff is a strong test of its ability to reproduce soil moisture, which is a far weaker function of precipitation. Third, our main findings depend on ranks (percentiles or deciles) of soil moisture rather than on absolute soil moistures. Soil moisture percentile ranks provide a reliable means of intercomparing different models and of defining drought indices (Luo and Wood 2007, 2008; Sheffield and Wood 2008). The AWAP system (Raupach et al. 2009) also uses percentile ranks for drought assessment. The greatest source of error in the soil moisture fields is likely to be associated with the gridded precipitation data, which are highly uncertain in the poorly gauged center of the Australian continent (Fig. 1b) but have much better reliability (Jones et al. 2009) in the southeastern part of the continent, which is the focus of this work.

3. Relative influences of ENSO and IOD on Australian hydrology

To understand the relative influences of the different ENSO–IOD categories on Australian hydrology, anomalies of precipitation and soil moisture are presented (Figs. 3 and 4). A two-tailed *t* test is used to determine the significance of spatial anomaly fields. This test estimates

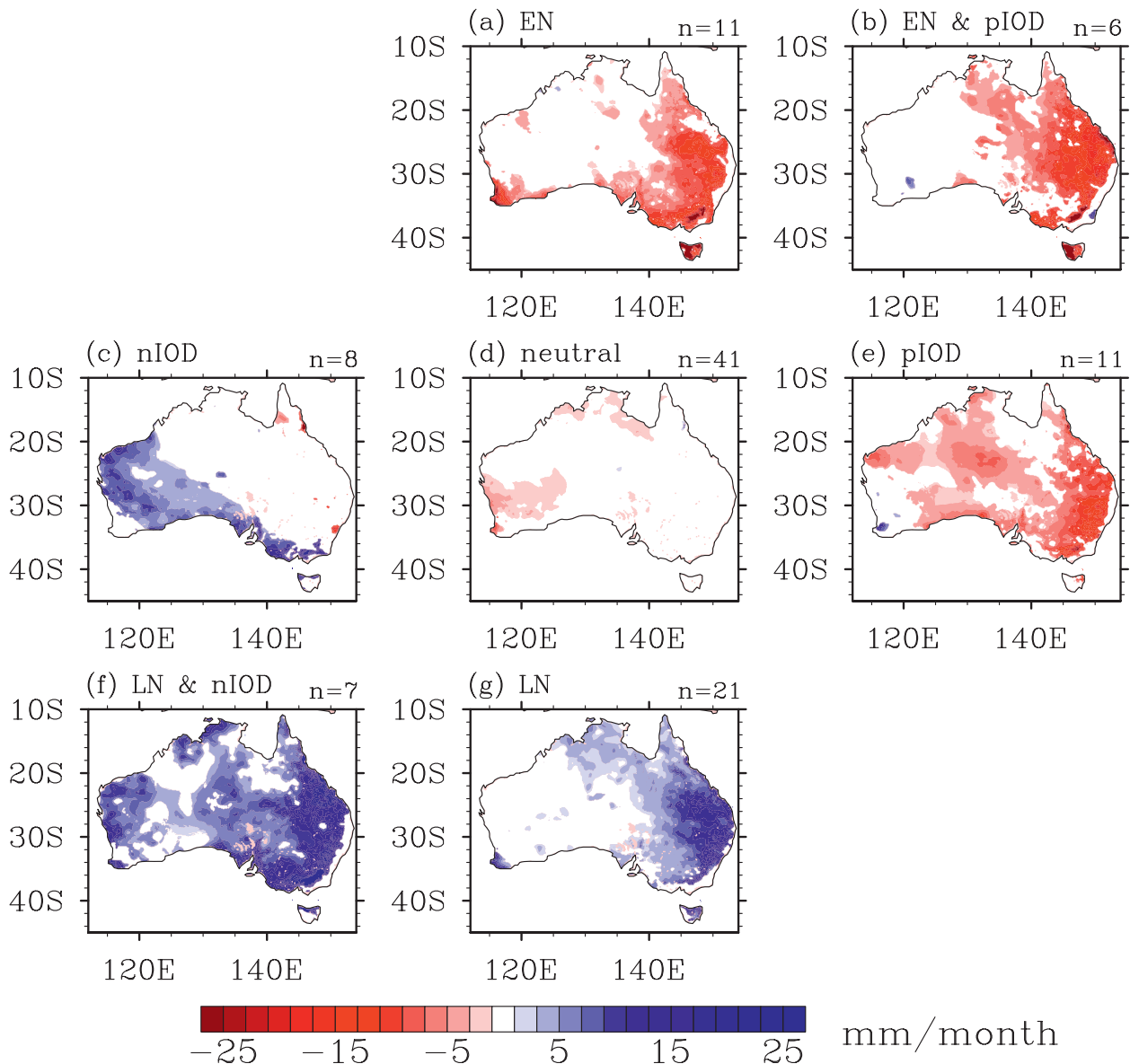


FIG. 3. Composite of the precipitation anomalies (mm month^{-1}) in the different ENSO-IOD categories with the number of members (n) in each category indicated; anomalies are for June–October over the period 1900–2006. Only anomalies are shown that are significant at the 80% confidence level as estimated by a two-tailed t test.

the statistical significance at which the composite mean in any one category is distinguishable from the mean of all years at each grid point.

a. Precipitation

Anomalous dry conditions dominate across the eastern half of Australia during years with El Niño, pIOD, and positive combined events (Figs. 3a, 3b, and 3e). Both the MDB and SSEA regions are characterized by lower rainfall in excess of 15 mm month^{-1} . Risbey et al. (2009a) associated this with a reduction in the

atmospheric thickness gradient forced by the SST anomalies east of Australia and a resultant weakening of the jet stream. This change in the background state is unfavorable for the development of cutoff low pressure systems that normally bring rain to the southeast (Pook et al. 2006). Tasmania experiences reductions in precipitation in excess of 20 mm month^{-1} during El Niño years (consistent with Hill et al. 2009) and positive combined events, while only the northeast of the island is affected during a pIOD (Fig. 3a). During El Niño years, significant reductions in rainfall are also seen for southwest Western Australia.

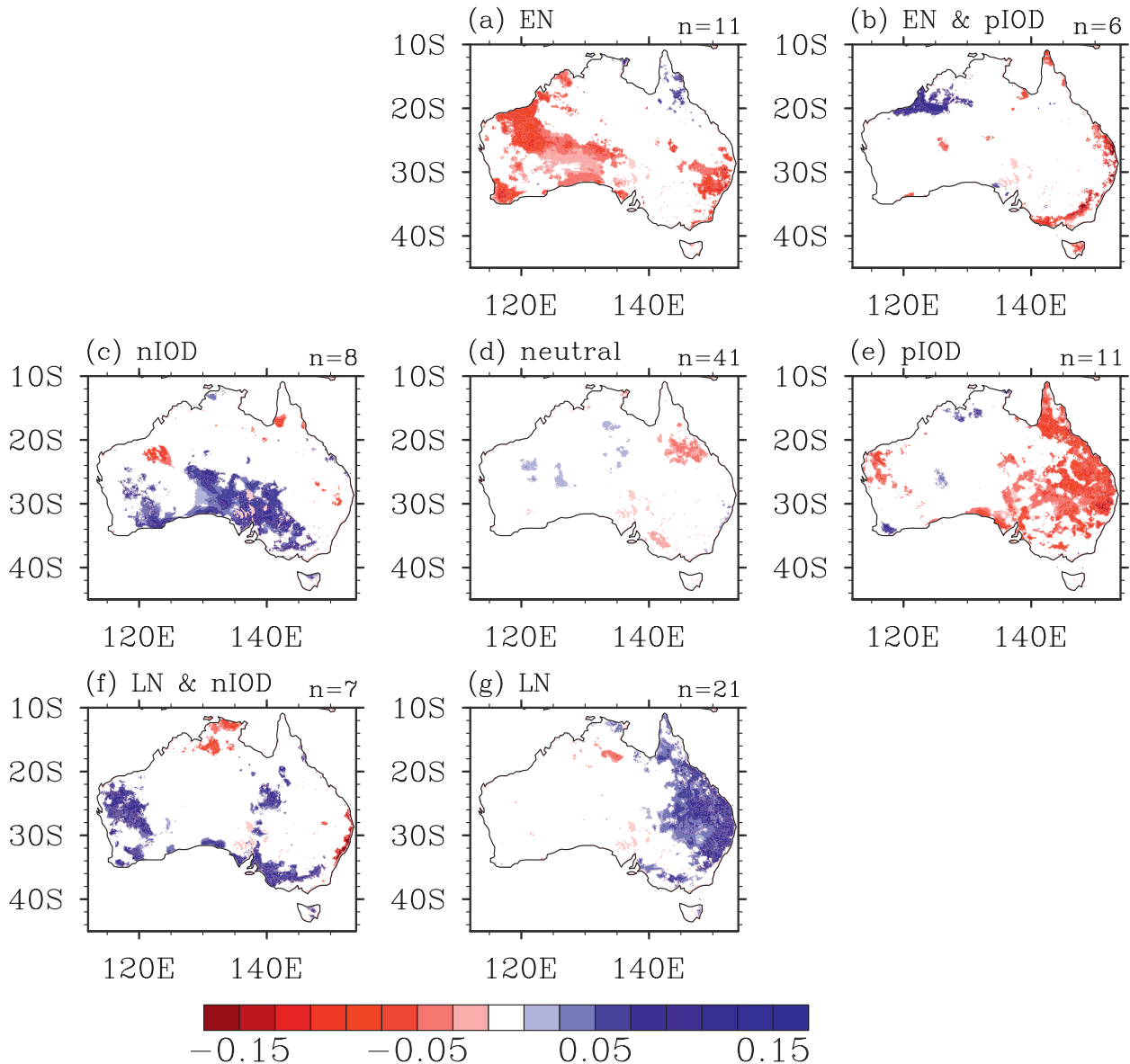


FIG. 4. Composite of the lower-layer soil moisture anomalies in the different ENSO–IOD categories with the number of members (n) in each category indicated; anomalies are for June–October over the period 1900–2006. Only anomalies are shown that are significant at the 80% confidence level as estimated by a two-tailed t test.

In contrast, wet conditions occur during nIOD, La Niña, and negative combined events (Figs. 3c, 3f, and 3g). During nIOD events, a region of above-average rainfall extends from the northwest to the southeast of the Australian continent (Fig. 3c). This has previously been linked to enhanced northwest cloud-band activity (Tapp and Barrel 1984), though the actual effectiveness of the northwest cloud bands in delivering the rainfall is still under debate. Increased tropical moisture advection has been noted during nIOD events (Ummenhofer et al. 2009a). An enhanced meridional thickness gradient

forced by the underlying SST anomalies results in a thermal wind response with strengthened onshore flow and consistent increases in precipitation across western and southern regions of Australia (Ummenhofer et al. 2009b). During combined negative events much of Australia is characterized by anomalous wet conditions, including the eastern half of Australia, parts of Western Australia, and northern regions of Tasmania (Fig. 3f). The MDB and SSEA regions receive increased precipitation in excess of 25 mm month^{-1} . For SSEA, years in this negative combined category consistently account for the

wettest periods (Ummerhofer et al. 2009a). La Niña events bring above-average rainfall over most of the eastern half of Australia (Fig. 3g). This is associated with a strengthened meridional thickness gradient, which enhances the jet stream locally via a thermal wind response (Risbey et al. 2009a). The synoptic situation is thus advantageous for development of rain-producing systems. However, the center of the largest anomalies during La Niña events is located more toward the northeast of Australia (Fig. 3g). The northern reaches of the MDB receive increased rainfall in excess of 15 mm month^{-1} , while the anomalies recorded for the southern MDB are much smaller and are inconsistent for SSEA.

Notably across the different categories, the eastern seaboard east of the Great Dividing Range does not show anomalies consistent with the wider eastern Australian region. This affects the densely populated coastal areas, including the greater metropolitan regions of Sydney and Brisbane. Precipitation there seems largely determined by regional circulation features independent of ENSO and IOD. Similarly, McBride and Nicholls (1983) found precipitation along the coastal fringe of the eastern seaboard to be only weakly correlated with the Southern Oscillation index during the June–November months for the period 1932–74.

b. Soil moisture

It is of interest to further track the propagation of the water received as precipitation through the terrestrial branch of the hydrological cycle. Water in the ground as soil moisture represents an important water reservoir with vital functions for agriculture and ecosystems. We investigate soil moisture content in two separate layers: a shallow upper layer and a deep lower layer (Raupach et al. 2009). Layer thicknesses vary spatially and range between 0 and 0.7 m (upper) and 0.5 and 1.9 m (lower).

The upper-layer soil moisture closely tracks precipitation for the different ENSO–IOD categories (figure not shown). The anomalously dry categories during El Niño, pIOD, and positive combined events show reductions in upper-layer soil moisture across the eastern half of Australia. In contrast, the wet categories of nIOD, La Niña, and negative combined events record increased upper-layer soil moisture content for southern and eastern regions of Australia. When investigating precipitation and soil moisture trends across eastern Australia from remote sensing data, Liu et al. (2009) observed similar patterns between rainfall and soil moisture trends, although the magnitudes were stronger in the soil moisture in their study. They found ENSO to be an important factor in modulating near-surface hydrology across

SEA. Here, we actually find that the strongest negative (positive) soil moisture anomalies over the SSEA and MDB regions are observed during positive (negative) combined events (figure not shown). This highlights the importance of assessing the state of both IOD and ENSO when investigating SEA hydrological conditions.

Anomalies of lower-layer soil moisture in the different ENSO–IOD categories show more localized regions with significant responses (Fig. 4). The signal during the El Niño, pIOD, and positive combined events still primarily show overall drier conditions. However, during El Niño events, significant dry soil moisture anomalies are only found locally over parts of Western Australia and northern New South Wales (Fig. 4a). During the positive combined years, only a small area in SSEA and along the eastern seaboard shows a significant positive response (Fig. 4b). On the other hand, pIOD events are associated with a pronounced reduction in lower-layer soil moisture across the eastern half of Australia, especially over the northeast (Fig. 4e). In contrast to the “dry” categories, the wet categories of nIOD, La Niña, and negative combined events show larger spatial extents of significant anomalies in lower-layer soil moisture. During nIOD events, significant enhanced lower-layer soil moisture occurs extensively over southern regions of Australia (Fig. 4c). The spatial extent is more confined to SSEA and parts of Western Australia during negative combined events (Fig. 4f). La Niña years record increased lower-layer soil moisture over the northeast of Australia (Fig. 4g).

As detailed previously, SEA has sustained considerable rainfall trends (e.g., Murphy and Timbal 2008, and references therein) and a better understanding of the factors modulating the hydrological cycle on seasonal to interannual and decadal time scales is desirable. For the remainder of the study, we therefore focus on the regions of SSEA (sections 4 and 5) and the MDB (section 6). Both regions experience distinctive variations in precipitation and soil moisture during ENSO and IOD events (Figs. 3 and 4).

4. Seasonal variability in SSEA

Both ENSO and IOD are most prominent during certain seasons, more so for the IOD, which is strongly phase locked to September–November (e.g., Meyers et al. 2007). It is therefore informative to explore the seasonal variations of the ENSO–IOD responses. Figures 5 and 6 show the seasonal cycle of SSEA-averaged precipitation and lower soil moisture separated for the different ENSO and IOD categories. The long-term seasonal cycle is reproduced in each panel as the thick black line. For each category, the mean seasonal cycle is shown (red

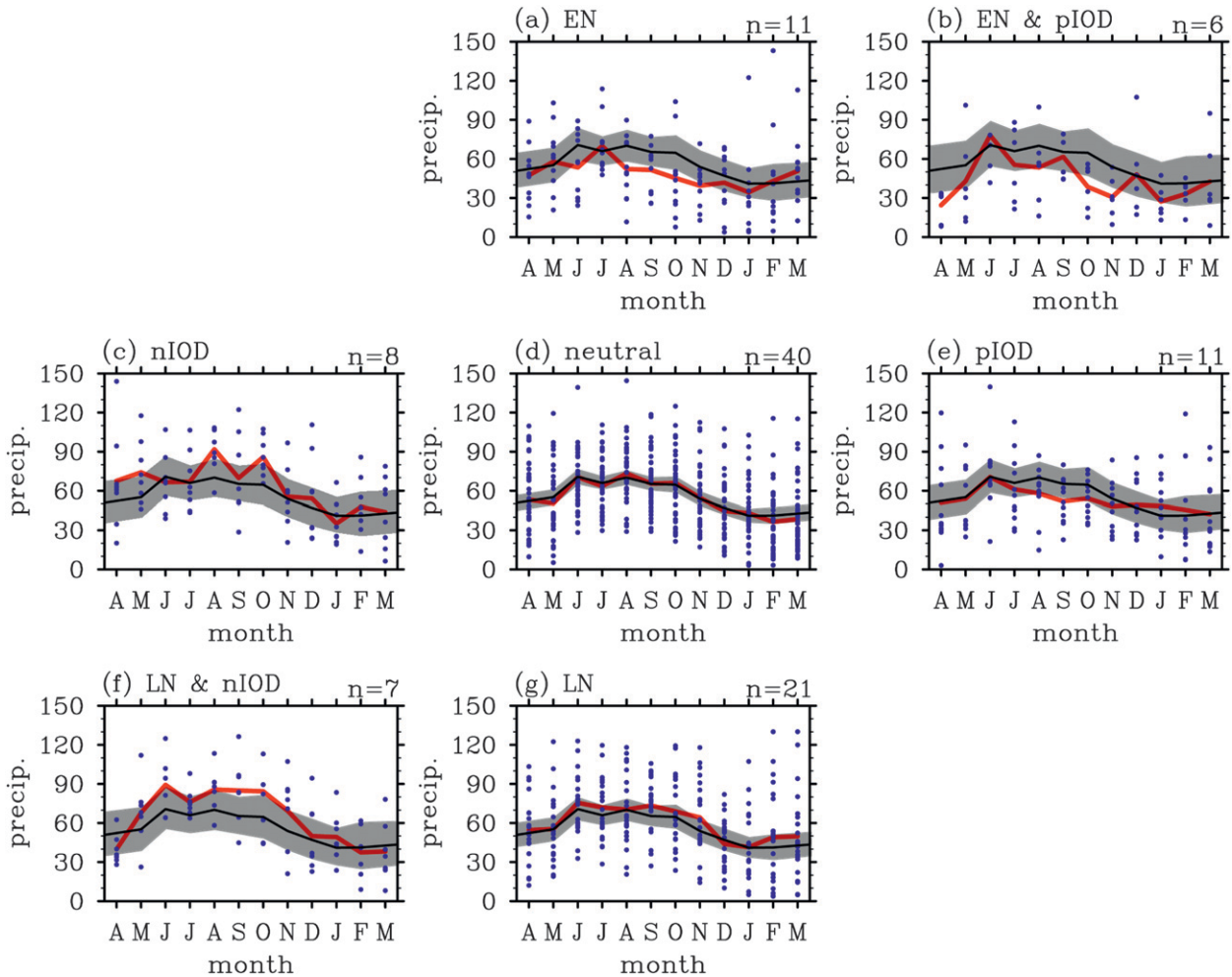


FIG. 5. Composite of the monthly SSEA precipitation (mm month^{-1}) in the different ENSO-IOD categories with the number of members (n) in each category indicated; the seasonal cycle from April to March is shown for the period 1900–2006. The black line reproduces the long-term seasonal cycle for all years. Within each category, individual years are shown with blue dots; the mean is indicated with a red line, and its 90% confidence levels by the gray shading, as determined by Monte Carlo testing. Where the red line lies outside the gray-shaded area, the values are significantly different from the long-term seasonal cycle.

line), along with the values recorded for individual years belonging to the various categories (blue dots).

To determine if the precipitation or soil moisture is significantly modified at different times of the year, a Monte Carlo test was used. For a given category, n represents the number of occurrences of that category. From all years (106 yr in total), we randomly picked n years and determined their mean seasonal cycle. This was repeated 25 000 times to produce a probability density function of expected precipitation/soil moisture by month. This could then be compared with precipitation/soil moisture associated with each category. The gray shading in Figs. 5 and 6 denotes the 5% and 95% lower and upper bounds of a 90% confidence interval for the randomly generated distribution. Note that this distribution differs depending on the number of members n , and

therefore the gray-shaded area varies between categories. Where the red line lies outside the gray-shaded area, the values are significantly different from the long-term seasonal cycle.

a. Precipitation

From Fig. 5, it is apparent that rainfall in SSEA generally peaks between June and October, averaging 67 mm month^{-1} , while the lowest values of 40 mm month^{-1} are recorded over austral summer. During El Niño years, significantly decreased mean rainfall occurs during August–November (Fig. 5a). This is a robust signal seen across most years in this category: less than 30% of El Niño years in September, or approximately 10% of El Niño years in November, exceed the long-term mean rainfall expected for that month.

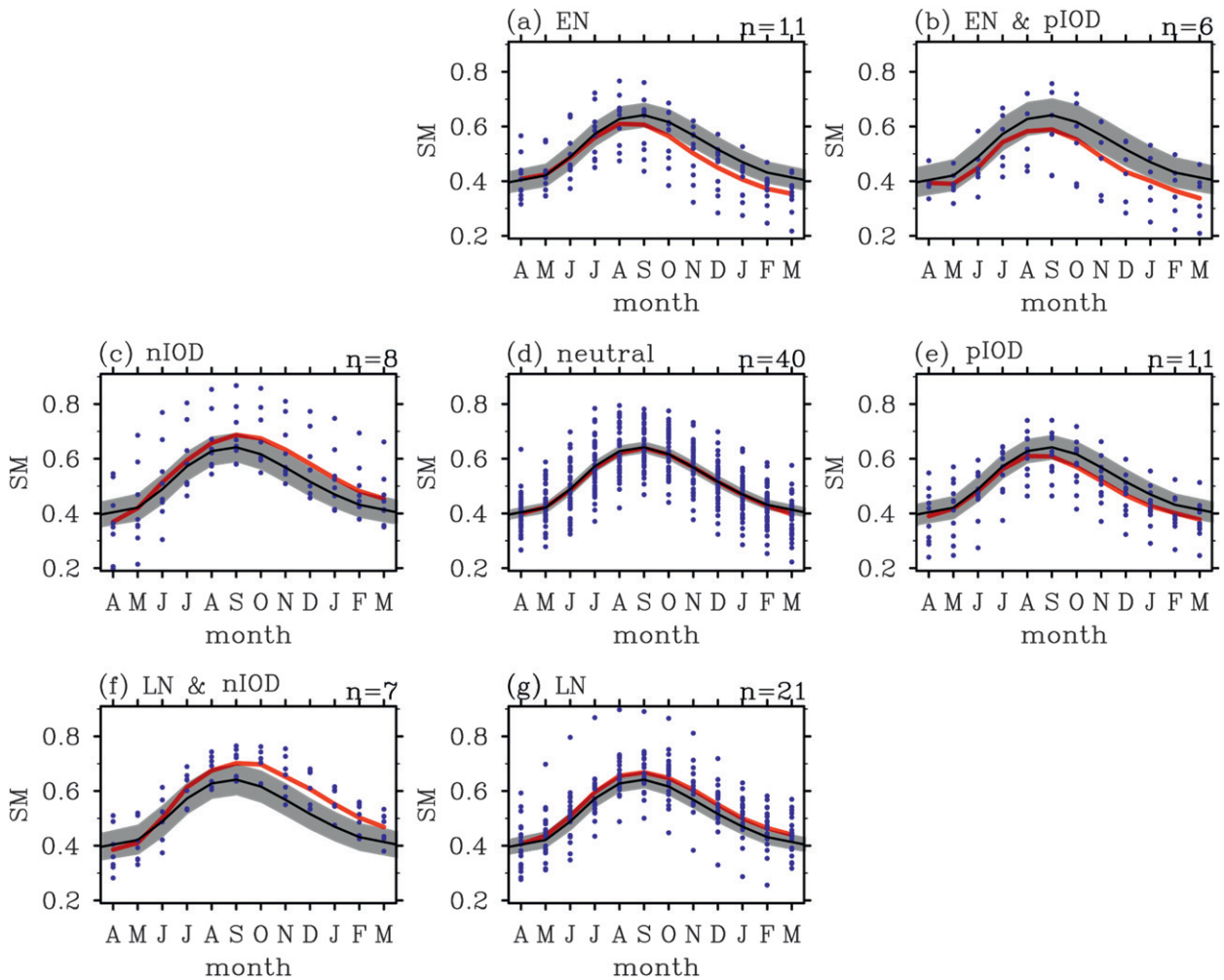


FIG. 6. Composite of the monthly SSEA lower-layer soil moisture in the different ENSO-IOD categories with the number of members (n) in each category indicated; the seasonal cycle from April to March is shown for the period 1900–2006. The black line reproduces the long-term seasonal cycle for all years. Within each category, individual years are shown with blue dots; the mean is indicated with a red line, and its 90% confidence levels by the gray shading, as determined by Monte Carlo testing. Where the red line lies outside the gray-shaded area, the values are significantly different from the long-term seasonal cycle.

Similarly, in the positive combined category very few events between August and January of the following year record above-average precipitation (Fig. 5b). During pIOD events, a significant decrease in rainfall is only recorded during August–October (Fig. 5e). However, a general tendency toward a lower number of months with wet conditions between July and November is observed in this category: less than 30% of pIOD years exceed the long-term mean precipitation during June–October.

For the wet categories nIOD, La Niña, and the negative combined events, the opposite can be observed, with generally enhanced cool-season rainfall (Figs. 5c, 5f, and 5g). During nIOD events, significantly above-average precipitation occurs during April–May, August, and

October, with the category's mean rainfall exceeding 90 mm month^{-1} in the latter 2 months (Fig. 5c). A notable reduction in the number of dry months during the May–October period is apparent. The negative combined events show anomalous wet conditions from May to November, which is significant for most of these months (Fig. 5f). Not a single month in this category records less than 40 mm month^{-1} between June and October. Instead, for June–September, more than 70% of the years in this category exceed the long-term mean rainfall expected, with many in excess of 90 mm month^{-1} .

On the other hand, despite many wet years in the category, La Niña events fail to show a consistent deviation from the expected long-term mean seasonal cycle (Fig. 5g). Only in 45%–60% of La Niña years does

the rainfall exceed the long-term mean expected for a given month. The only exception is September, when 70% of La Niñas record above-average precipitation. Gallant and Karoly (2009) described unusual conditions over SEA during the La Niña of 2007, with winter rainfall 35% below average and maximum temperatures 1.26°C above average. Based on past variability, they concluded that only 2% of La Niña events were likely to have this combined precipitation and temperature anomaly over the southern regions of the MDB and suggested modulating influences by the pIOD during 2007. From our analyses, the rainfall anomaly for 2007 is not unusual for La Niña events. However, the maximum temperature anomaly is anomalously high (figure not shown). It therefore seems that the low probability of only 2% for the combined anomalies during a La Niña year (Gallant and Karoly 2009) is largely due to the maximum temperature, not the precipitation. However, it should be noted that the regions investigated do not completely coincide.

b. Soil moisture

The seasonal cycle in soil moisture in the lower layer is also analyzed during the different ENSO–IOD categories for SSEA. Figure 6 reveals a pronounced seasonal cycle in the lower-layer soil moisture: soil moisture is highest in August–October, lowest in February–April. As such, there is an approximate 2-month lag between the maximum and minimum in the soil moisture relative to the precipitation. This is consistent with results from a cross-correlation analysis between precipitation and lower-layer soil moisture using monthly values over SSEA for the period 1900–2006, which showed a maximum correlation of 0.5 (p value ≤ 0.001) at 2-month lag (figure not shown).

The dry categories of El Niño, pIOD, and positive combined events show a significant decrease in lower-layer soil moisture for September–March of the following year (Figs. 6a, 6b, and 6e). Of all the El Niño years, only 30% exceed the long-term mean soil moisture expected in October, while this drops to only 10% for December–February. Similarly, only 20% of pIOD events for November–January and less than 35% of positive combined events for September–March exceed the long-term mean soil moisture values.

Significant increases in soil moisture are recorded during nIOD, La Niña, and negative combined events for the second half of the year (Figs. 6c, 6f, and 6g). In the nIOD and negative combined events, no dry events based on soil moisture occur until December after September and July, respectively (Figs. 6c and 6f). From June onward, in excess of 60% of La Niña years exceed the average expected soil moisture for a given month (Fig. 6g).

However, again a considerable number of dry events are still evident in the La Niña category. This highlights the inconsistent signal in precipitation anomalies over SSEA associated with La Niña events (see Fig. 5g; Ummenhofer et al. 2009a).

5. Interannual versus decadal influences in SSEA

Given the presence of prominent precipitation and soil moisture anomalies over SSEA associated with ENSO and IOD during the second half of the year, the remainder of the study focuses on the June–October months. We investigate the historic record of average precipitation and soil moisture over SSEA for the June–October months during the period 1900–2006 and its association with ENSO and IOD events (Fig. 7). For precipitation, the years were ranked according to the amount of rainfall received and divided into deciles. Extreme dry and wet years were defined as years in the lowest and highest decile (i.e., each containing 11 yr). The same procedure was followed for upper and lower soil moisture results.

For precipitation, extreme dry years in SSEA largely coincided with El Niño (3 times), pIOD (2 times), or positive combined years (1 time). However, one La Niña and several neutral years were also associated with anomalous dry conditions. On the other hand, extreme wet conditions occurred during La Niña (3 times), nIOD (1 time), or negative combined years (3 times). One pIOD (1923) and one positive combined event (1991) coincided with anomalously wet conditions. Overall, a surprisingly good separation into the dry and wet categories can be seen, associated with below- and above-average precipitation in SSEA (Fig. 7a).

The upper-layer soil moisture anomalies closely follow the precipitation (figure not shown). However, the largest positive soil moisture anomalies occurred after several years of above-average rainfall: this was the case in the mid-1950s when several high-rainfall years culminated in 1956 in the largest positive upper-layer soil moisture anomaly seen in the record. A similar effect was observed for the nIOD in 1974, following the above-average rainfall associated with La Niña in the previous year. This cumulative effect is seen more clearly in the lower soil moisture anomalies (Fig. 7b). For example, a pIOD in 1913 resulted in a negative anomaly in both precipitation and upper-layer soil moisture, but no signal was apparent in the lower-layer soil moisture. The following year, an even larger decrease in precipitation associated with the El Niño of 1914 occurred, reflected also by a large deficit in lower-layer soil moisture. The years 1915–17 saw enhanced precipitation associated with an nIOD and two negative combined events (Fig. 7a).

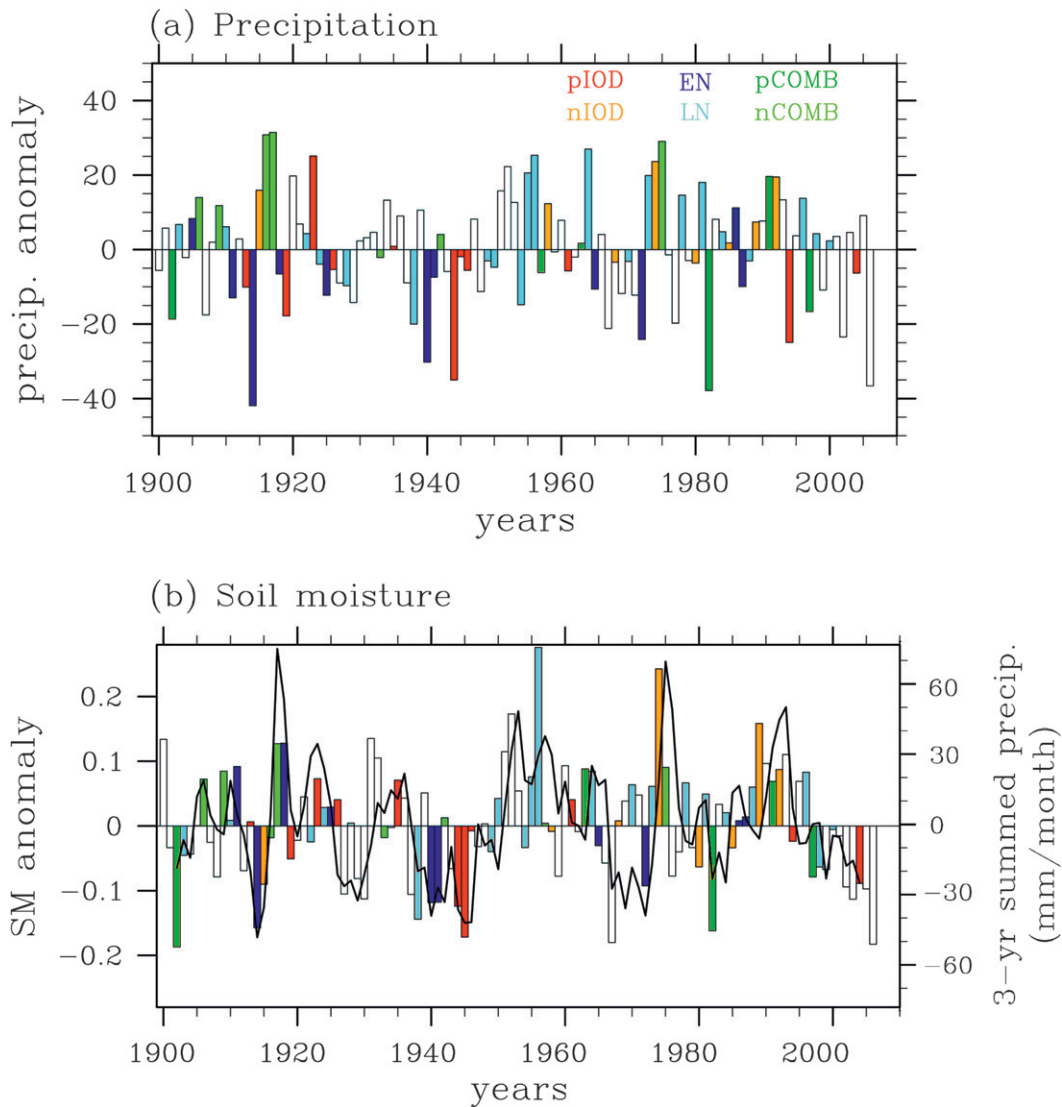


FIG. 7. Anomalies of SSEA (a) precipitation (mm month^{-1}) and (b) lower-layer soil moisture over SSEA with the associated ENSO-IOD categories indicated in color; all anomalies are for June–October over the period 1900–2006. The black line in (b) represents the precipitation summed over the preceding 3 yr (mm month^{-1}).

However, lower-layer soil moisture only reached positive values in 1917, following 2 years of above-average rainfall (Fig. 7b). In other words, several high-rainfall years were required to overcome the lower-layer soil moisture deficit of 1914. Similarly, the large positive anomalies in lower-layer soil moisture of 1956, 1974, and 1989 followed a period of above-average rainfall. On the other hand, prolonged periods of below-average precipitation and resultant droughts were clearly recorded in the lower-layer soil moisture, for example, during the 1920s, the World War II drought, and the Big Dry (Fig. 7b). The black line in Fig. 7b shows a running 3-yr sum (for the previous 3 years) of precipitation. The close match

between this summed precipitation and lower-layer soil moisture demonstrates how the lower-layer soil moisture essentially acts as a natural low-pass filter. The 3-yr summed precipitation fairly closely tracks the lower-layer soil moisture throughout the past century (Fig. 7b). In those few places where it does not track the soil moisture, the disagreement is likely explained by the presence of anomalously high rainfall in the months preceding the June–October period. Anomalous rainfall then is not recorded in the June–October rainfall total, but does influence June–October soil moisture.

In addition to the interannual variations in precipitation and soil moisture associated with ENSO and IOD

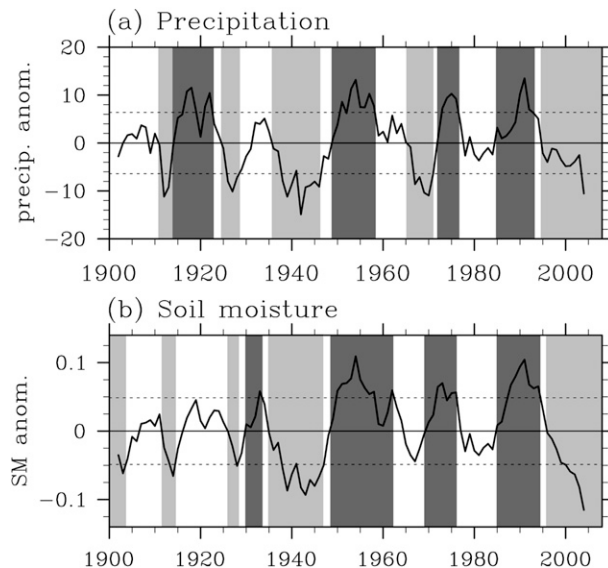


FIG. 8. Time series of 5-yr running means of SSEA (a) precipitation (mm month^{-1}) and (b) lower-layer soil moisture anomalies for June–October over the period 1900–2006. Years defined as prolonged dry (wet) periods are shaded in light gray (dark gray).

events, the historical record also shows prolonged periods of anomalous dry or wet conditions (Fig. 8). Such multiyear periods, so-called intervals, are defined on the 5-yr running mean of the time series. A dry or wet interval is defined to occur when the 5-yr running mean exceeds a cutoff value of ± 1 standard deviation. The starting point of an interval was taken as the year when the 5-yr running mean crossed zero prior to the point of exceeding the cutoff. The interval's endpoint occurred when the 5-yr running mean fell consistently below or above the cutoff. In addition to incorporating the extreme conditions at the height of a dry or wet period, this definition also includes the years leading *into* it. The lengths of intervals can vary from 2–3 years to a decade or longer.

Over the past century, SSEA has experienced several dry and wet intervals of differing duration and severity (shaded regions in Fig. 8). The dry intervals seen in the precipitation included the short, but severe, dry years of 1913–14, the mid-1920s, the World War II drought (1936–46), the late 1960s, and the present Big Dry (post-1994; Fig. 8a). The dry periods were interspersed by prolonged stretches of above-average rainfall over SSEA: 1914–22, the 1950s, the mid-1970s, and 1985–92.

The dry and wet intervals in the soil moisture record were defined as described for the precipitation and similar dry/wet periods can be seen. Dry periods in the soil moisture included the end of the Federation drought, 1912–14, the mid-1920s, the World War II drought, and the Big Dry (Fig. 8b). Wet intervals based on soil moisture occurred in the 1950s, early 1960s, 1970s, and the

mid-1980s to early 1990s. Some of the shorter and less intense periods of enhanced or reduced precipitation are not captured in the lower-layer soil moisture. However, the severity of the Big Dry becomes apparent in the soil moisture record, rivaling the soil moisture deficits sustained during the World War II drought. Recent higher air temperatures and the resultant increases in evaporation are thought to contribute to the drought's severity (Nicholls 2004; Cai and Cowan 2008b).

It is of interest to contrast the relative influences of ENSO and IOD for SSEA over interannual and decadal time scales. For this, we used the years in the highest and lowest deciles (i.e., 11 wettest and driest years in the time series; Fig. 7) and the years defined as wet and dry intervals (i.e., periods highlighted in Fig. 8). For each set of years, the number of occurrences of the different ENSO–IOD categories was determined. In Fig. 9, the circles indicate the actual number of events in the given ENSO–IOD category that are associated with the wet and dry conditions defined on deciles and intervals, respectively. To determine whether the event frequency is unusual, for each category, a bootstrapping technique was used to generate an expected distribution based on random events using all years. The box-and-whiskers plots in Fig. 9 summarize these expected distributions for each category. From the bootstrapping method, each actual event also has an error bar associated with it. If the error bar of the actual event does not overlap with the box or whiskers, then the number of events is significantly different from a sample based on all years at the 98% confidence level. This analysis was conducted for the time series of precipitation and lower-layer soil moisture.

To test the robustness of the results, the analyses were also repeated for the shorter record post-1950 where there is improved data quality (figures not shown). The results are qualitatively similar; however, statistically robust results across all the different categories can only be obtained when including the full record. We therefore restrict further discussion to the full data record, under the assumption that the early record still provides useful information.

For wet conditions based on SSEA precipitation deciles, significant increases in negative combined events are found (Fig. 9a). In the dry decile, El Niño years are seen more often than normal. This agrees with previous results (cf. Figs. 3 and 7; Ummenhofer et al. 2009a). For the wet and dry conditions based on precipitation intervals (Fig. 9b), the relative ENSO–IOD influences are very different: wet intervals are characterized by a reduced frequency of pIOD and increases in the number of nIOD events. The high number of nIOD events is especially prominent, with 75% of all nIOD events

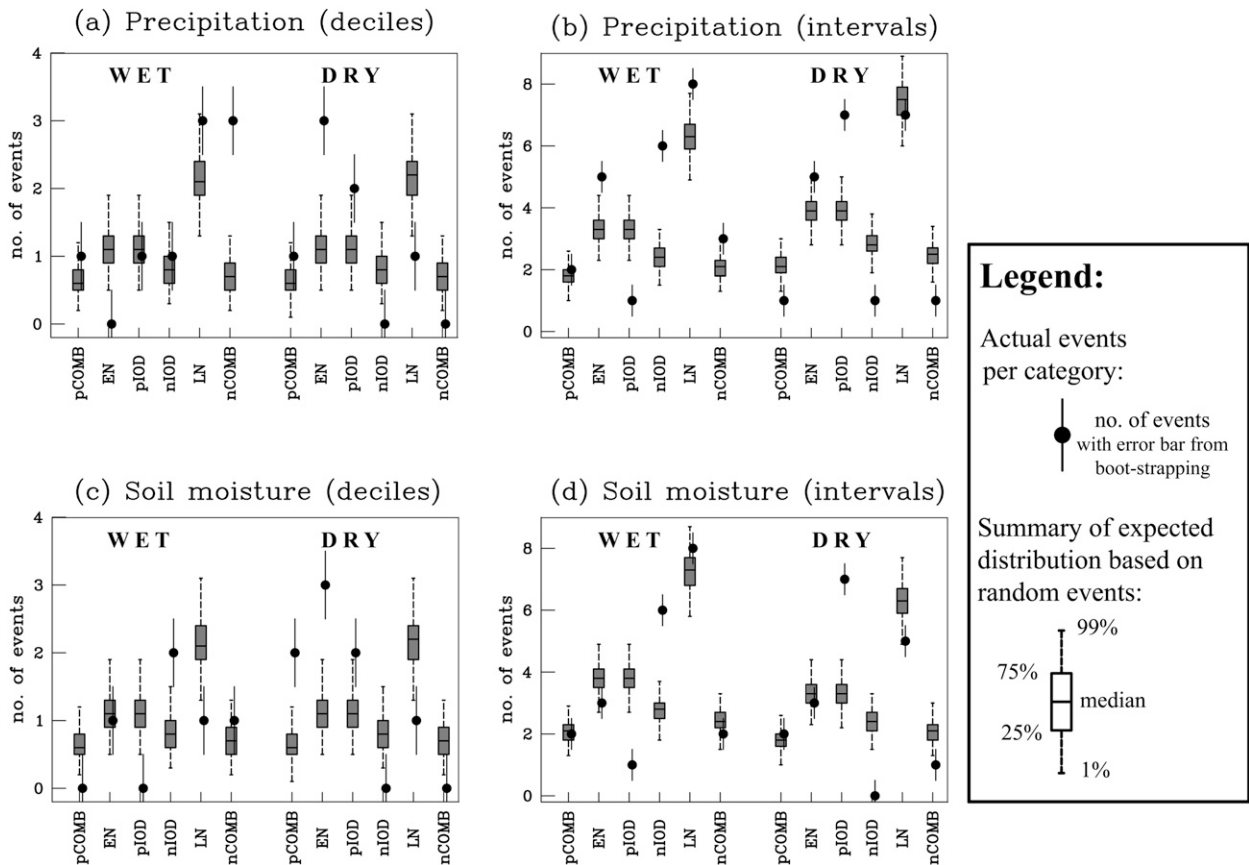


FIG. 9. Circles (with corresponding boot strapped error bars) indicate the actual number of events in the given ENSO–IOD category that are associated with wet and dry conditions based on (a),(b) precipitation and (c),(d) lower-layer soil moisture over the SSEA for the period 1900–2006. Dry and wet conditions are dependent on (left) upper and lower deciles and (right) intervals, respectively. To determine whether the event frequency is unusual, for each category, a boot strapping technique is used to generate an expected distribution based on random events using all years. The box-and-whiskers plot summarizes this expected distribution. If the error bar of the actual event does not overlap with the box or whisker, then the number of events is significantly different from a sample based on all years at the 98% confidence level.

occurring during wet intervals. Wet intervals also show marginally significant increases in El Niño years. Dry intervals experience a reduced number of negative combined and nIOD years, while significantly more pIOD events are recorded. For the dry intervals, it is surprising to see that El Niño years, which were present in significantly enhanced numbers when considering the lower decile, are no longer significantly different.

These results become even more apparent when comparing the interannual and decadal ENSO–IOD influences based on soil moisture. Anomalies in the lower-layer soil moisture show lower-frequency variability compared to the higher-frequency anomalies in precipitation. This is also reflected in the frequency of ENSO and IOD events associated with anomalous lower-layer soil moisture. During dry deciles of lower-layer soil moisture, increased numbers of positive combined and

El Niño events are recorded (Fig. 9c). Based on the analysis of intervals, lower-layer soil moisture wet and dry conditions are associated with significantly modified numbers of IOD events, while ENSO events remain unchanged (Fig. 9d). Wet intervals show unusually few pIOD events and a significantly enhanced number of nIOD, with more than 85% of all nIODs occurring during wet intervals. In dry intervals, an unusually high number of pIOD events are recorded with in excess of 63% of all pIOD events occurring during these times. The opposite is seen for the nIOD with not a single nIOD event during any dry interval.

In summary, Fig. 9 suggests that ENSO seems to modify SSEA water availability on interannual time scales, but less so on decadal scales. On decadal time scales, the IOD’s influence is more robust, where the number of both positive and negative IOD events is significantly

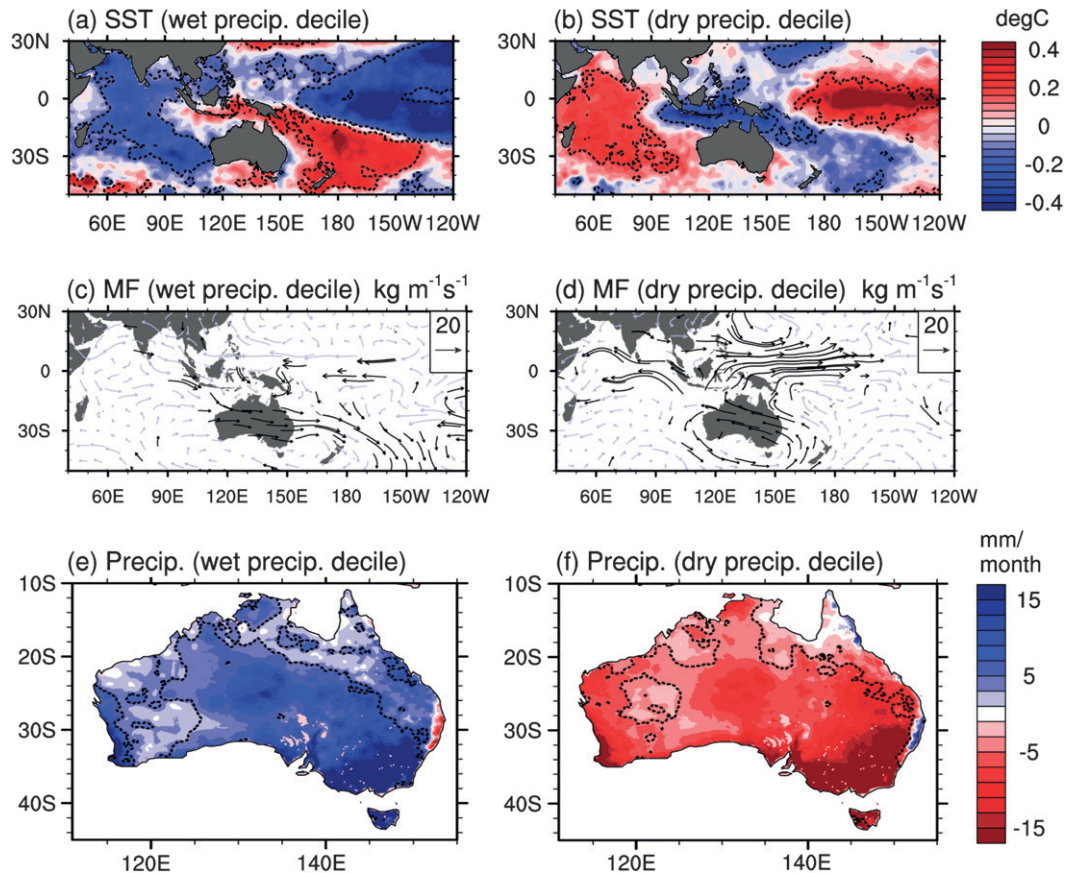


FIG. 10. Composite of the anomalies in (a),(b) SST ($^{\circ}\text{C}$), (c),(d) moisture flux (vertically integrated below 500 hPa; in $\text{kg m}^{-1} \text{s}^{-1}$), and (e),(f) precipitation (mm month^{-1}) during extreme (right) upper and (left) lower 10% of years as determined by SSEA precipitation; all anomalies are for June–October over the period 1900–2006 (except moisture flux, which covers only the period 1948–2006). The area enclosed by the dashed contours denotes anomalies that are significant at the 90% confidence level as estimated by a two-tailed t test.

changed from the expected distribution during both dry and wet intervals (Figs. 9b and 9d). Power et al. (1999b) also found decadal variability in the Indian Ocean to be associated with significant variations in precipitation across eastern Australia. The decadal component of Indian Ocean SST that they linked to eastern Australian rainfall exhibited a strong signal south of 40°S . This is, however, well south of the typical IOD SST pattern. Thus, Power et al.'s (1999b) mechanism for driving decadal variability seems, at first glance, to be inconsistent with the IOD as a dominant driver. To investigate this further, we analyze the spatial patterns of key oceanic and atmospheric variables for dry and wet conditions in SSEA for both interannual and decadal time scales.

Composites of SSEA dry and wet conditions are presented in Figs. 10 and 11, based on deciles for precipitation and for lower-layer soil moisture, respectively. As described previously, the precipitation deciles are representative of the interannual variability, while lower-layer

soil moisture focuses on low-frequency variability and a decadal signal, acting as a natural low-pass filter on precipitation. During wet years based on SSEA precipitation deciles, central tropical and subtropical Indian Ocean SSTs are anomalously cool by in excess of -0.4°C , while the ocean to the north of Australia shows slightly above-average temperatures (Fig. 10a). In contrast during dry years, warm SST anomalies of more than 0.4°C above average are seen over the western and central tropical and subtropical Indian Ocean, with a strong cooling of the same magnitude observed to the north of Australia around Indonesia (Fig. 10b). The central equatorial Pacific is anomalously cool (warm) during wet (dry) SSEA years, with SST anomalies of opposite sign in the subtropical South Pacific. For the wet SSEA years, the SST anomalies show features of both an nIOD in the Indian Ocean and a La Niña in the Pacific. The opposite is true for the dry years. The SSTs are thus broadly consistent with the signature seen during negative and positive

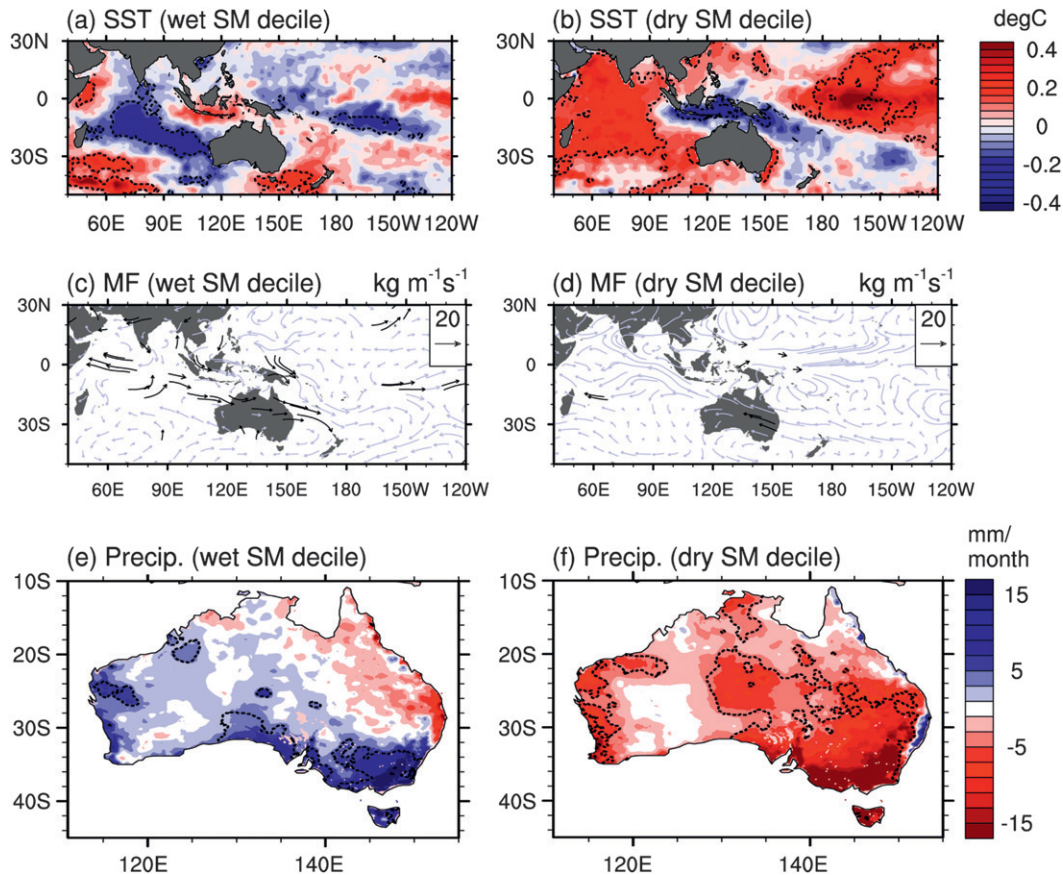


FIG. 11. Composite of the anomalies in (a),(b) SST ($^{\circ}\text{C}$), (c),(d) moisture flux (vertically integrated below 500 hPa; in $\text{kg m}^{-1}\text{s}^{-1}$), and (e),(f) precipitation (mm month^{-1}) during extreme (right) upper and (left) lower 10% of years as determined by SSEA lower-layer soil moisture; all anomalies are for June–October over the period 1900–2006 (except for moisture flux, which covers only the period 1948–2006). The area enclosed by the dashed contours denotes anomalies that are significant at the 90% confidence level as estimated by a two-tailed t test.

combined events. This can be understood as the very wettest and driest years largely occur during combined ENSO and IOD events (Ummenhofer et al. 2009a).

During wet (dry) SSEA years, an enhanced (reduced) meridional gradient in SST across the eastern Indian Ocean is set up. This was shown to change the overlying atmospheric thickness, leading to a thermal wind response with an increase (decrease) in westerly onshore flow onto the Australian continent during wet (dry) years (Ummenhofer et al. 2008). This is manifest in an increased moisture flux (integrated below 500 hPa) from northwest Australia to the southeast during wet SSEA years (Fig. 10c). For dry SSEA years, a reduction in northwesterly moisture flux is seen, while a large westerly anomaly in moisture flux is observed over the western Pacific warm pool region associated with the anomalous Pacific SST pattern (Fig. 10d). Over the Pacific, Risbey et al. (2009a) found that the SST anomalies during negative (positive) combined events modulated

the atmospheric thickness, strengthening (weakening) the jet stream and leading to enhanced (weakened) cutoff low pressure systems over eastern Australia. The precipitation pattern across Australia is characterized by anomalously wet and dry conditions across large parts of the continent (Figs. 10e and 10f), consistent with the respective circulation anomalies. Years based on SSEA precipitation deciles thus seem to show features spatially coherent across large parts of Australia.

These patterns are quite different for composites based on SSEA lower-layer soil moisture. During high-moisture conditions, the magnitude of the SST anomalies over the Pacific Ocean and the spatial extent of significant anomalies are noticeably reduced (Fig. 11a). In contrast, the Indian Ocean shows large areas of significant SST anomalies: cool anomalies in the central subtropical region, and warm anomalies in the southwestern Indian Ocean and to the north of Australia. This SST pattern with its “tripolar” structure is reminiscent

of a dominant mode of Indian Ocean variability (Santoso 2005; D. Dommenget 2009, personal communication), with certain features of this discussed previously for observations (e.g., Nicholls 1989; Stretten 1983; England et al. 2006) and for climate model simulations (e.g., Frederiksen and Balgovind 1994; Ummenhofer et al. 2008). During dry conditions based on soil moisture, anomalous warm (cool) conditions over the western (eastern) Indian Ocean are observed, while the central equatorial Pacific also records above-average temperatures (Fig. 11b).

The moisture flux anomalies associated with wet (dry) SSEA soil moisture conditions show enhanced (reduced) westerly moisture advection onto Australia (Figs. 11c and 11d). However, the spatial extent of significant anomalies is limited, most likely due to the short data record available for NNR. The region of significant precipitation anomalies is much more closely confined: during wet soil moisture conditions, above-average rainfall in excess of 15 mm month^{-1} is recorded for SEA south of 30°S and east of 130°E (i.e., including SSEA), parts of Western Australia, and Tasmania (Fig. 11e). The situation is reversed during dry SSEA soil moisture conditions, but the anomalies extend farther north to include much of the MDB region (Fig. 11f).

To summarize Figs. 10 and 11, interannual variability in SSEA is influenced by both Pacific and Indian Ocean conditions associated with ENSO and the IOD, respectively. Induced by SST anomalies during combined positive (negative) events in the Indo-Pacific region, changes in the atmospheric circulation result in extreme dry (wet) conditions over SSEA and more broadly over large parts of Australia. In contrast, decadal variability over SSEA seems to be linked more robustly to the Indian Ocean. The decadal Indian Ocean pattern contains a combined signal of tropical and subtropical variability, reminiscent of a dominant mode of Indian Ocean variability. Decadal variations (Ashok et al. 2004; Tozuka et al. 2007) and long-term trends (Abram et al. 2008; Ihara et al. 2008; Cai et al. 2009) in Indian Ocean surface properties are therefore likely to play a significant role in modulating Australian precipitation on these time scales. Over Australia, the decadal signal in precipitation is confined more locally to the SSEA region (Figs. 11e and 11f) than the interannual signal (Figs. 10e and 10f). However, for both time scales an asymmetry is apparent between dry and wet conditions, with dry responses extending farther north into the MDB. This will be discussed further in the next section.

6. Murray–Darling Basin

Given the large difference in the dominant drivers of water availability between interannual and decadal time

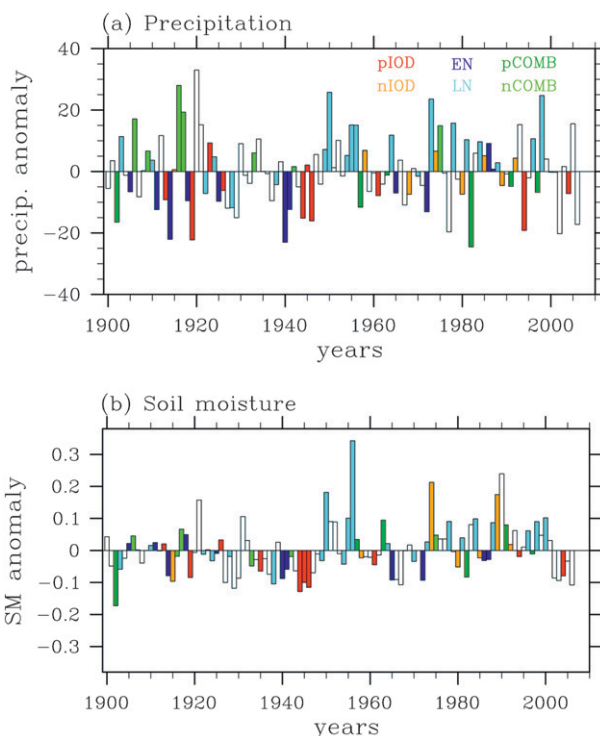


FIG. 12. Anomalies of MDB (a) precipitation (mm month^{-1}) and (b) lower-layer soil moisture over MDB with the associated ENSO–IOD categories indicated in color; all anomalies are for June–October over the period 1900–2006.

scales for SSEA, it is of interest to understand whether our results are particular to this region or common for other areas as well. We therefore repeat key analyses for the MDB region, which has also recently sustained considerable decreases in precipitation (Murphy and Timbal 2008, and references therein).

For the MDB region (see Fig. 1a), interannual variations in precipitation and soil moisture are also intricately linked to Indo-Pacific variability associated with ENSO and the IOD (Risbey et al. 2009b). The June–October anomalies in MDB precipitation and lower-layer soil moisture are given in Fig. 12, together with the ENSO–IOD classification. Extreme dry years in the MDB are associated with El Niño (2 times), pIOD (4 times), and positive combined (2 times) events, while extreme wet conditions occurred during La Niña (4 times) and negative combined (3 times) events (Fig. 12a). Upper-layer soil moisture anomalies are very similar to the ones defined for precipitation (figure not shown). However, La Niña events become much more dominant, with more than 60% of wet years coinciding with a La Niña. For La Niña years, Risbey et al. (2009a) described an enhanced meridional thickness gradient across eastern Australia, leading to a strengthening of the jet stream.

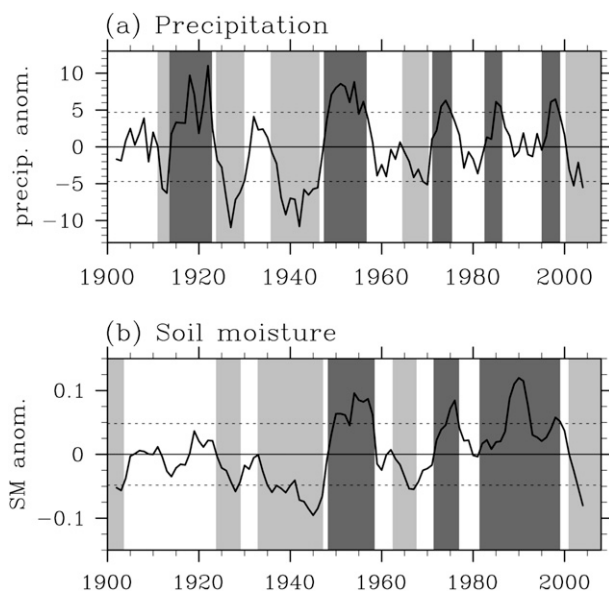


FIG. 13. Time series of 5-yr running means of MDB (a) precipitation (mm month^{-1}) and (b) lower-layer soil moisture anomalies for June–October over the period 1900–2006. Years defined as prolonged dry (wet) periods are shaded in light gray (dark gray).

This is favorable for cutoff low pressure system development and increased rainfall over the MDB region.

As seen for SSEA, the lower-layer soil moisture in the MDB emphasizes low-frequency variations in water availability (Fig. 12b). Compared to the high-frequency interannual variability seen in precipitation and upper-layer soil moisture, there are much-lower-frequency changes in the lower soil moisture. Prolonged periods of wet conditions were seen from the mid-1970s to 2000, while sustained deficits in soil moisture dominated from the mid-1920s to the mid-1940s, including the severe World War II drought and during the recent Big Dry.

These prolonged periods of dry and wet conditions appear in the time series of 5-yr running means for precipitation and lower-layer soil moisture (Fig. 13). The MDB intervals were defined in the same way as described for the SSEA. Based on precipitation deficits, droughts in the MDB occurred during 1911–13, the mid-1920s, 1936–46, the late 1960s, and post-2000 (Fig. 13a). The severity and duration of the iconic World War II drought is particularly apparent. The dry conditions were interspersed with periods of above-average precipitation, including 1914–22, 1948–56, the early 1970s, the mid-1980s, and the late 1990s.

Based on lower-layer soil moisture, prolonged dry conditions dominated during the Federation drought at the turn of the last century, in the mid-1920s, during the World War II drought (1933–46), in the 1960s, and post-2001 (Fig. 13b). Extended wet intervals occurred

throughout the 1950s and, except for a few individual years, almost continuously from 1972 to 1997. In the lower-layer soil moisture record, the World War II drought, following shortly after the dry conditions of the mid-1920s, seems exceptional in its severity and especially in its duration. The prolonged above-average soil moisture content sustained throughout the late 1980s and early 1990s is also unusual in the MDB record.

We contrast the relative influences of ENSO and IOD for interannual and lower-frequency time scales, following the same methodology outlined for SSEA. For wet conditions, based on MDB precipitation deciles, significant increases in La Niña and negative combined events are recorded (Fig. 14a). In the dry decile, positive combined and pIOD years are seen more often than expected, while the number of La Niña events is significantly reduced. For wet intervals, increased numbers of La Niña events are seen, while pIOD events occur less frequently (Fig. 14b). During dry intervals, the number of positive combined events is significantly reduced, while unusually high numbers of pIOD events occur. Based on lower-layer soil moisture deciles, only La Niña events appear in unusually low (high) numbers for extreme dry (wet) years (Fig. 14c). In contrast for the intervals, the frequency of both positive and negative IOD events is significantly changed (Fig. 14d). The latter highlights the importance of the IOD at decadal time scales for prolonged soil drought conditions for the MDB region.

In summary, the MDB region is significantly influenced by both La Niña and IOD events. In particular, La Niña plays a much more prominent role than for SSEA, especially on interannual time scales and for prolonged wet periods. For longer-term variability associated with prolonged dry and wet periods, the number of pIOD events is significantly changed from the expected distribution. This is consistent with previous results (cf. Fig. 3).

7. Summary and conclusions

We have investigated the relative influences of ENSO and IOD for Australian hydrology on seasonal to interannual and decadal time scales using observations, reanalysis data, and hindcasts of soil moisture. Emphasis was placed on two regions in southeastern Australia, namely, SSEA and the MDB region, both of which have recently suffered prolonged drought conditions. A primary aim of the study was to determine whether the drivers of interannual variability are the same as the drivers of longer-term, decadal variability, with a focus on the predominant rainfall period during the cool season (June–October).

The results highlight the importance of examining both Indian and Pacific Ocean variability patterns in

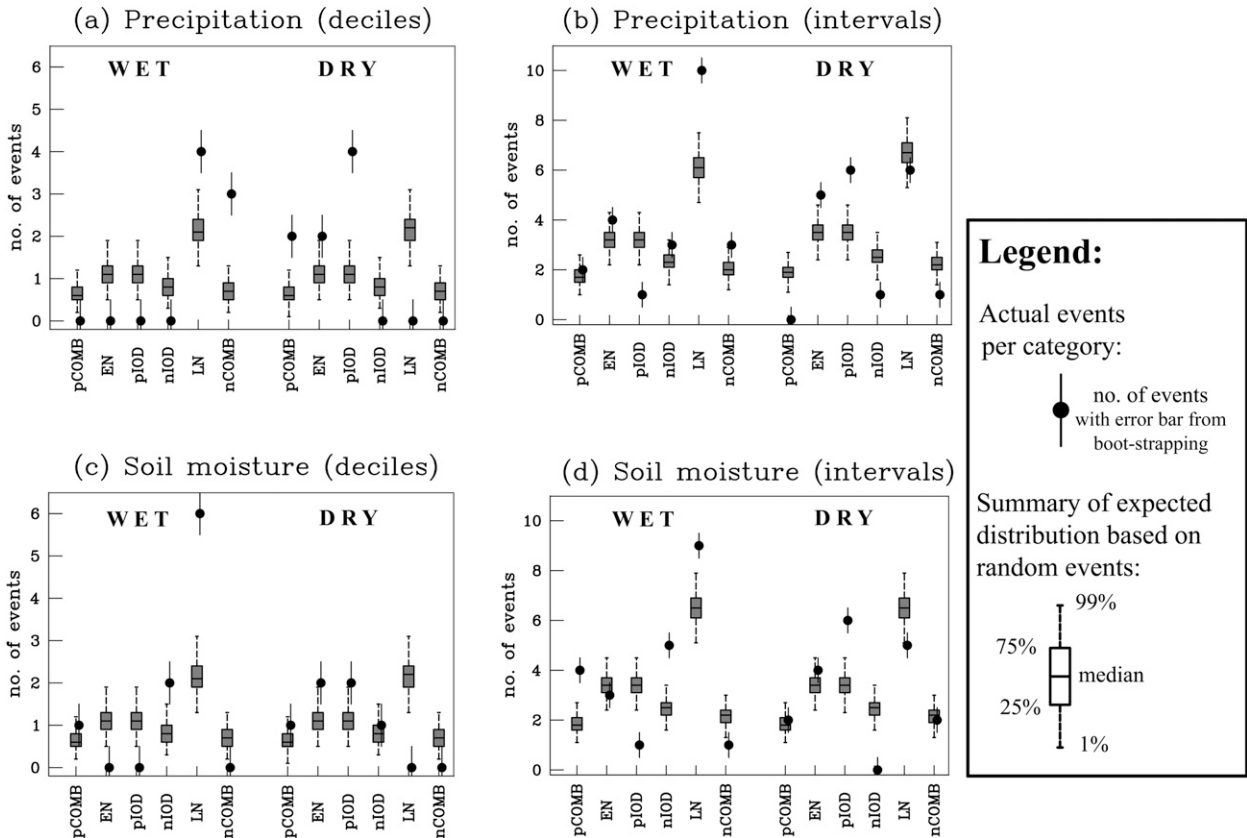


FIG. 14. Circles (with corresponding boot strapped error bars) indicate the actual number of events in the given ENSO–IOD category that are associated with wet and dry conditions based on (a),(b) precipitation and (c),(d) lower-layer soil moisture over the MDB for the period 1900–2006. Dry and wet conditions are dependent on upper and lower (left) deciles and (right) intervals, respectively. To determine whether the event frequency is unusual, for each category, a boot strapping technique is used to generate an expected distribution based on random events using all years. The box-and-whiskers plot summarizes this expected distribution. If the error bar of the actual event does not overlap with the box or whisker, then the number of event is significantly different from a sample based on all years at the 98% confidence level.

assessing their impacts on Australian hydrology. In other words, we treat the full tropical Indo-Pacific region with two distinct modes of variability that interact on different time scales. For example, the impacts of a La Niña event will be very different when one co-occurs with an nIOD, while the other does not. The same is true for other combinations of drivers. Care must also be taken in assessing opposite phases of ENSO and IOD. For example, the impacts of El Niño are not a mirror image of those seen during a La Niña (Power et al. 2006). This is even more apparent in the case of positive and negative phases of the IOD. Linear analyses (e.g., correlation analyses) will alias such nonlinearities and potentially hide important and highly distinct features exhibited by opposite phases (Risbey et al. 2009b). Furthermore, the impacts associated with combined ENSO and IOD events are not simply a linear combination of the impacts associated with pure events. For example, the sum

of the rainfall anomalies seen during an nIOD event and a La Niña is quite different from that observed during a combined negative event (figure not shown). This is true, albeit to a lesser degree, for positive combined events. As pointed out by Meyers et al. (2007), Australian rainfall is very sensitive to small changes in the SST patterns across the Indo-Pacific region.

For both SSEA and the MDB, distinct differences are seen in the relative influences of ENSO and IOD on interannual and lower-frequency time scales. For SSEA, El Niño modulates water availability on interannual time scales, but not on a decadal scale. On decadal time scales, Indian Ocean variability provides a more robust explanation for prolonged dry and wet periods than do Pacific conditions. For the MDB region on interannual time scales, the influence of La Niña events is more significant than for SSEA. On decadal time scales the situation becomes less clear: pIOD events occur in

unusual numbers for prolonged dry and wet periods, for both the precipitation- and soil-moisture-based analyses. In contrast, the frequency of nIOD events is only unusual for soil moisture. Based on both precipitation and soil moisture, La Niña events are unusually frequent during prolonged wet periods, but La Niña frequency is not unusual for dry periods. Thus, for the MDB region, as for SSEA, distinct differences are seen in what drives an individual dry or wet year compared to a prolonged period with dry or wet conditions.

These results have important implications for choosing the appropriate technique/methodology to analyze decadal to longer-term variations. It raises interesting questions on how to investigate, for example, multiyear droughts and cautions against the use of statistical techniques that assume a linear response. Previous work voiced concerns in regard to low-frequency variations in ENSO characteristics, in the relationships between SST and regional rainfall, and in particular the implications for the statistical analysis techniques employed (e.g., Gershunov et al. 2001; Wittenberg 2009). Given the large degree of noise in the climate system, the limited availability of high-quality multidecadal observational records, in particular in the Southern Hemisphere, poses serious challenges for climate impact research at decadal time scales and beyond. A concerted effort, based on a combination of observations, reanalyses/hindcasts, and climate model simulations, is required to develop an improved understanding of nonlinear interactions of modes of variability and their impacts on the hydrological cycle on decadal and longer time scales.

As pointed out by LeBlanc et al. (2009), the hydrological drought across SEA continued despite the return to average rainfall conditions in 2007. Here, we have shown that it is a lack of extreme wet conditions associated with nIOD events and a higher proportion of pIOD events that characterizes multiyear droughts over SSEA. So, the return to average rainfall has not been sufficient to break the current drought. After a return to average rainfall, there is a delay in the response of runoff and streamflow because increased precipitation first has to replenish the depleted soil moisture store. This is evident in runoff and discharge rates remaining at very low levels despite average rainfall in 2007.

The Indo-Pacific climate system has sustained considerable trends over recent decades. Observed changes have been associated with the dominant climate modes in the two ocean basins, namely, ENSO (Power and Smith 2007) and the IOD (Abram et al. 2008; Ihara et al. 2008; Cai et al. 2009). With these two climate modes intricately linked to regional circulation across different time scales, changes in the characteristics of both ENSO and IOD have the potential to significantly affect the climate

over the surrounding landmasses. For example, trends in IOD frequency have been related to a changed East Asian monsoon (Abram et al. 2008) and southern Australian rainfall declines (Cai et al. 2009). Given the observed and projected changes in dominant drivers of SEA climate, the present work highlights how the dominant influences of the Indian and Pacific Ocean differ between interannual and multiyear time scales for water-stressed regions in Australia's southeast.

Acknowledgments. Use of the following observational and reanalysis products is gratefully acknowledged: NCEP–NCAR reanalysis and NOAA_ERSSST_V2 SST data provided by NOAA/OAR/ESRL/PSD, Boulder, Colorado, through their Web site (<http://www.cdc.noaa.gov>), and the ERA-40 data developed by the European Centre for Medium-Range Weather Forecasting. An earlier version of the manuscript benefited from helpful suggestions by Andrew Marshall, Andrea Taschetto, and three anonymous reviewers. This work was supported by the Australian Research Council. The contributions of P. R. Briggs and M. R. Raupach were funded by the South Eastern Australian Climate Initiative.

REFERENCES

- ABARE, 2009: The impact of climate change on the irrigated agricultural industries in the Murray-Darling Basin. Australian Bureau of Agricultural and Resource Economics Conf. Paper 09.3, 17 pp.
- Abram, N. J., M. K. Gagan, J. E. Cole, W. S. Hantoro, and M. Mudelsee, 2008: Recent intensification of tropical climate variability in the Indian Ocean. *Nat. Geosci.*, **1**, 849–853, doi:10.1038/ngeo357.
- Arblaster, J. M., G. A. Meehl, and A. M. Moore, 2002: Interdecadal modulation of Australian rainfall. *Climate Dyn.*, **18**, 519–531.
- Ashok, K., Z. Guan, and T. Yamagata, 2003: Influence of the Indian Ocean dipole on the Australian winter rainfall. *Geophys. Res. Lett.*, **30**, 1821, doi:10.1029/2003GL017926.
- , W.-L. Chun, T. Motoi, and T. Yamagata, 2004: Decadal variability of the Indian Ocean dipole. *Geophys. Res. Lett.*, **31**, L24207, doi:10.1029/2004GL021345.
- , S. K. Behera, S. A. Rao, H. Weng, and T. Yamagata, 2007: El Niño Modoki and its possible teleconnection. *J. Geophys. Res.*, **112**, C11007, doi:10.1029/2006JC003798.
- Brown, J. N., P. C. McIntosh, M. J. Pook, and J. S. Risbey, 2009: An investigation of the links between ENSO flavors and rainfall processes in southeastern Australia. *Mon. Wea. Rev.*, **137**, 3786–3795.
- Cai, W., and T. Cowan, 2008a: Dynamics of late autumn rainfall reduction over southeastern Australia. *Geophys. Res. Lett.*, **35**, L09708, doi:10.1029/2008GL033727.
- , and —, 2008b: Evidence of impacts from rising temperatures on inflows to the Murray–Darling Basin. *Geophys. Res. Lett.*, **35**, L07701, doi:10.1029/2008GL033390.
- , —, and A. Sullivan, 2009: Recent unprecedented skewness towards positive Indian Ocean dipole occurrences and their

- impact on Australian rainfall. *Geophys. Res. Lett.*, **36**, L11705, doi:10.1029/2009GL037604.
- CSIRO, 2010: Program annual report 2009–10. South Eastern Australian Climate Initiative (SEACI), CSIRO, 101 pp. [Available online at <http://www.csiro.au/resources/Annual-Report-2009-10.html>.]
- D'Arrigo, R., N. Abram, C. Ummenhofer, J. Palmer, and M. Mudelsee, 2011: Reconstructed streamflow for Citarum River, Java, Indonesia: Linkages to tropical climate dynamics. *Climate Dyn.*, **36**, 451–462.
- Drosowsky, W., and M. Williams, 1991: The Southern Oscillation in the Australian region. Part I: Anomalies at the extremes of the oscillation. *J. Climate*, **4**, 619–638.
- England, M. H., C. C. Ummenhofer, and A. Santoso, 2006: Interannual rainfall extremes over southwest Western Australia linked to Indian Ocean climate variability. *J. Climate*, **19**, 1948–1969.
- Frederiksen, C. S., and R. C. Balgobind, 1994: The influence of the Indian Ocean/Indonesian SST gradient on the Australian winter rainfall and circulation in an atmospheric GCM. *Quart. J. Roy. Meteor. Soc.*, **120**, 923–952.
- Gallant, A. J. E., and D. J. Karoly, 2009: Atypical influence of the 2007 La Niña on rainfall and temperature in southeastern Australia. *Geophys. Res. Lett.*, **36**, L14707, doi:10.1029/2009GL039026.
- Gershunov, A., N. Schneider, and T. Barnett, 2001: Low-frequency modulation of the ENSO–Indian monsoon rainfall relationship: Signal or noise? *J. Climate*, **14**, 2486–2492.
- Hendon, H. H., D. W. J. Thompson, and M. C. Wheeler, 2007: Australian rainfall and surface temperature variations associated with the Southern Hemisphere annular mode. *J. Climate*, **20**, 2452–2467.
- Hill, K. J., A. Santoso, and M. H. England, 2009: Interannual Tasmanian rainfall variability associated with large-scale climate modes. *J. Climate*, **22**, 4383–4397.
- Hope, P., B. Timbal, and R. Fawcett, 2009: Associations between rainfall variability in the southwest and southeast of Australia and their evolution through time. *Int. J. Climatol.*, **30**, 1360–1371, doi:10.1002/joc.1964.
- Ihara, C., Y. Kushnir, and M. A. Cane, 2008: Warming trend of the Indian Ocean SST and Indian Ocean dipole from 1880 to 2004. *J. Climate*, **21**, 2035–2046.
- Jones, D. A., W. Wang, and R. Fawcett, 2009: High-quality spatial climate data-sets for Australia. *Aust. Meteor. Oceanogr. J.*, **58**, 233–248.
- Kalnay, E., and Coauthors, 1996: The NCEP/NCAR 40-Year Reanalysis Project. *Bull. Amer. Meteor. Soc.*, **77**, 437–471.
- Karoly, D. J., and K. Braganza, 2005: Attribution of recent temperature changes in the Australian region. *J. Climate*, **18**, 457–464.
- Kistler, R., and Coauthors, 2001: The NCEP–NCAR 50-Year Reanalysis: Monthly means CD-ROM and documentation. *Bull. Amer. Meteor. Soc.*, **82**, 247–267.
- LeBlanc, M. J., P. Tregoning, G. Ramillien, S. O. Tweed, and A. Fakes, 2009: Basin-scale, integrated observations of the early 21st century multiyear drought in southeast Australia. *Water Resour. Res.*, **45**, W04408, doi:10.1029/2008WR007333.
- Liang, X., 1994: A two-layer variable infiltration capacity land surface representation for general circulation models. Water Resources Series Tech. Rep. TR140, University of Washington, Seattle, WA, 208 pp.
- , D. P. Lettenmaier, E. F. Wood, and S. J. Burges, 1994: A simple hydrologically based model of land-surface water and energy fluxes for general-circulation models. *J. Geophys. Res.*, **99**, 14 415–14 428.
- Liu, Y. Y., A. I. J. M. van Dijk, R. A. M. de Jeu, and T. R. H. Holmes, 2009: An analysis of spatiotemporal variations of soil and vegetation moisture from a 29-year satellite derived data set over mainland Australia. *Water Resour. Res.*, **45**, W07405, doi:10.1029/2009WR007187.
- Luo, L. F., and E. F. Wood, 2007: Monitoring and predicting the 2007 U.S. drought. *Geophys. Res. Lett.*, **34**, L22702, doi:10.1029/2007GL031673.
- , and —, 2008: Use of Bayesian merging techniques in a multimodel seasonal hydrologic ensemble prediction system for the eastern United States. *J. Hydrometeorol.*, **9**, 866–884.
- McBride, J. L., and N. Nicholls, 1983: Seasonal relationships between Australian rainfall and the Southern Oscillation. *Mon. Wea. Rev.*, **111**, 1998–2004.
- McIntosh, P. C., M. J. Pook, J. S. Risbey, S. N. Lisson, and M. Rebbeck, 2007: Seasonal climate forecasts for agriculture: Towards better understanding and value. *Field Crops Res.*, **104**, 130–138, doi:10.1016/j.fcr.2007.03.019.
- McKenzie, N. J., and J. Hook, 1992: Interpretations of the Atlas of Australian Soils. CSIRO Division of Soils Tech. Rep. 94/1992, Canberra, ACT, Australia, 7 pp.
- , D. W. Jacquier, L. J. Ashton, and H. P. Cresswell, 2000: Estimation of soil properties using the Atlas of Australian Soils. CSIRO Land and Water Tech. Rep. 11/00, Canberra, ACT, Australia, 24 pp.
- Meneghini, B., I. Simmonds, and I. N. Smith, 2007: Association between Australian rainfall and the southern annular mode. *Int. J. Climatol.*, **27**, 109–121.
- Meyers, G., P. McIntosh, L. Pigot, and M. Pook, 2007: The years of El Niño, La Niña, and interactions with the tropical Indian Ocean. *J. Climate*, **20**, 2872–2880.
- Mpelasoka, F., K. Hennessy, R. Jones, and B. Bates, 2008: Comparison of suitable drought indices for climate change impacts assessment over Australia towards resource management. *Int. J. Climatol.*, **28**, 1283–1292.
- Murphy, B. F., and B. Timbal, 2008: A review of recent climate variability and climate change in southeastern Australia. *Int. J. Climatol.*, **28**, 859–879.
- Nicholls, N., 1988: More on early ENSOs: Evidence from Australian documentary sources. *Bull. Amer. Meteor. Soc.*, **69**, 4–6.
- , 1989: Sea surface temperatures and Australian winter rainfall. *J. Climate*, **2**, 965–973.
- , 2004: The changing nature of Australian droughts. *Climatic Change*, **63**, 323–336.
- , 2006: Detecting and attributing Australian climate change: A review. *Aust. Meteor. Mag.*, **55**, 199–211.
- , 2009: Local and remote causes of the southern Australian autumn–winter rainfall decline, 1958–2007. *Climate Dyn.*, **34**, 835–845, doi:10.1007/s00382-009-0527-6.
- Pook, M., P. C. McIntosh, and G. A. Meyers, 2006: The synoptic decomposition of cool season rainfall in the southeastern Australian cropping region. *J. Appl. Meteor. Climatol.*, **45**, 1156–1170.
- Power, S., and I. N. Smith, 2007: Weakening of the Walker circulation and apparent dominance of El Niño both reach record levels, but has ENSO really changed? *Geophys. Res. Lett.*, **34**, L18702, doi:10.1029/2007GL030854.
- , T. Casey, C. Folland, A. Colman, and V. Mehta, 1999a: Interdecadal modulation of the impact of ENSO on Australia. *Climate Dyn.*, **15**, 319–324.

- , F. Tseitkin, V. Mehta, B. Lavery, S. Torok, and N. Holbrook, 1999b: Decadal climate variability in Australia during the twentieth century. *Int. J. Climatol.*, **19**, 169–184.
- , M. Haylock, R. Colman, and X. Wang, 2006: The predictability of interdecadal changes in ENSO activity and ENSO teleconnections. *J. Climate*, **19**, 4755–4771.
- Raupach, M. R., 2000: Equilibrium evaporation and the convective boundary layer. *Bound.-Layer Meteor.*, **96**, 107–141.
- , P. R. Briggs, V. Haverd, E. A. King, M. Paget, and C. M. Trudinger, 2009: Australian Water Availability Project (AWAP): CSIRO Marine and Atmospheric Research Component: Final Report for Phase 3. CAWCR Tech. Rep. 013, Canberra, ACT, Australia, 67 pp.
- Rayner, N. A., D. E. Parker, E. B. Horton, C. K. Folland, L. V. Alexander, and D. P. Rowell, 2003: Global analyses of SST, sea ice and night marine air temperature since the late nineteenth century. *J. Geophys. Res.*, **108**, 4407, doi:10.1029/2002JD002670.
- Risbey, J. S., M. J. Pook, P. C. McIntosh, C. C. Ummenhofer, and G. Meyers, 2009a: Variability of synoptic features associated with cool season rainfall in southeastern Australia. *Int. J. Climatol.*, **29**, 1595–1613.
- , —, —, M. C. Wheeler, and H. H. Hendon, 2009b: On the remote drivers of rainfall variability in Australia. *Mon. Wea. Rev.*, **137**, 3233–3253.
- Ropelewski, C. F., and M. S. Halpert, 1987: Global and regional scale precipitation patterns associated with El Niño–Southern Oscillation. *Mon. Wea. Rev.*, **115**, 1606–1626.
- Saji, N. H., B. N. Goswami, P. N. Vinayachandran, and T. Yamagata, 1999: A dipole mode in the tropical Indian Ocean. *Nature*, **401**, 360–363.
- Santos, A., 2005: Evolution of climate anomalies and variability of Southern Ocean water masses on interannual to centennial timescales. Ph.D. thesis, University of New South Wales, 326 pp.
- Sheffield, J., and E. F. Wood, 2008: Global trends and variability in soil moisture and drought characteristics, 1950–2000, from observation-driven simulations of the terrestrial hydrologic cycle. *J. Climate*, **21**, 432–458.
- Sohn, E., 2007: The Big Dry. *Sci. News*, **172**, 17.
- Streten, N. A., 1983: Extreme distributions of Australian annual rainfall in relation to sea surface temperature. *J. Climatol.*, **3**, 143–153.
- Tapp, R. G., and S. L. Barrel, 1984: The north-west Australian cloud band: Climatology, characteristics and factors associated with development. *Int. J. Climatol.*, **4**, 411–424.
- Taschetto, A. S., and M. H. England, 2009: El Niño Modoki impacts on Australian rainfall. *J. Climate*, **22**, 3167–3174.
- , C. C. Ummenhofer, A. Sen Gupta, and M. H. England, 2009: Effect of anomalous warming in the central Pacific on the Australian monsoon. *Geophys. Res. Lett.*, **36**, L12704, doi:10.1029/2009GL038416.
- Tozuka, T., J.-J. Luo, S. Masson, and T. Yamagata, 2007: Decadal modulations of the Indian Ocean dipole in the SINTEX-F1 coupled GCM. *J. Climate*, **20**, 2881–2894.
- Ummenhofer, C. C., A. Sen Gupta, M. J. Pook, and M. H. England, 2008: Anomalous rainfall over southwest Western Australia forced by Indian Ocean sea surface temperatures. *J. Climate*, **21**, 5113–5134.
- , M. H. England, G. A. Meyers, P. C. McIntosh, M. J. Pook, J. S. Risbey, A. Sen Gupta, and A. S. Taschetto, 2009a: What causes southeast Australia's worst droughts? *Geophys. Res. Lett.*, **36**, L04706, doi:10.1029/2008GL036801.
- , A. Sen Gupta, A. S. Taschetto, and M. H. England, 2009b: Modulation of Australian precipitation by meridional gradients in east Indian Ocean sea surface temperature. *J. Climate*, **22**, 5597–5610.
- Uppala, S. M., and Coauthors, 2005: The ERA-40 Re-Analysis. *Quart. J. Roy. Meteor. Soc.*, **131**, 2961–3012.
- Vecchi, G. A., and B. J. Soden, 2007: Global warming and the weakening of the tropical circulation. *J. Climate*, **20**, 4316–4340.
- , —, A. T. Wittenberg, I. M. Held, A. Leetmaa, and M. J. Harrison, 2006: Weakening of tropical Pacific atmospheric circulation due to anthropogenic forcing. *Nature*, **441**, 73–76.
- Wang, G., and H. Hendon, 2007: Sensitivity of Australian rainfall to inter-El Niño variations. *J. Climate*, **20**, 4211–4226.
- Webster, P. J., A. M. Moore, J. P. Loschnigg, and R. R. Leben, 1999: Coupled ocean–atmosphere dynamics in the Indian Ocean during 1997–98. *Nature*, **401**, 356–360.
- Weng, H., K. Ashok, S. K. Behera, S. A. Rao, and T. Yamagata, 2007: Impacts of recent El Niño Modoki on dry/wet conditions in the Pacific Rim during boreal summer. *Climate Dyn.*, **29**, 113–129.
- Wittenberg, A. T., 2009: Are historical records sufficient to constrain ENSO simulations? *Geophys. Res. Lett.*, **36**, L12702, doi:10.1029/2009GL038710.
- Zhang, L., K. Hickel, W. R. Dawes, F. H. S. Chiew, A. W. Western, and P. R. Briggs, 2004: A rational function approach for estimating mean annual evapotranspiration. *Water Resour. Res.*, **40**, W02502, doi:10.1029/2003WR002710.